

Quantum and Boltzmann transport in a quasi-one-dimensional wire with rough edges

J. Feilhauer and M. Moško*

Institute of Electrical Engineering, Slovak Academy of Sciences, 841 04 Bratislava, Slovakia

(Received 19 November 2010; revised manuscript received 21 March 2011; published 30 June 2011)

We study electron transport in quasi-one-dimensional metallic wires. Our aim is to compare an impurity-free wire with rough edges with a smooth wire with impurity disorder. We calculate the electron transmission through the wires by the scattering-matrix method, and we find the Landauer conductance for a large ensemble of disordered wires. We first study the impurity-free wire whose edges have roughness with a correlation length comparable with the Fermi wavelength. Simulating wires with the number of the conducting channels (N_c) as large as 34–347, we observe the roughness-mediated effects which are not observable for small N_c (~ 3 –9) used in previous works. First, we observe the crossover from the quasi-ballistic transport to the diffusive one, where the ratio of the quasi-ballistic resistivity to the diffusive resistivity is $\sim N_c$ independent of the parameters of roughness. Second, we find that transport in the diffusive regime is carried by a small effective number of open channels, equal to ~ 6 . This number is universal—independent of N_c and of the parameters of roughness. Third, we see that the inverse mean conductance rises linearly with the wire length (a sign of the diffusive regime) up to the length twice larger than the electron localization length. We develop a theory based on the weak-scattering limit and semiclassical Boltzmann equation, and we explain the first and second observations analytically. For the impurity disorder we find a standard diffusive behavior. Finally, we derive from the Boltzmann equation the semiclassical electron mean free path and we compare it with the quantum mean free path obtained from the Landauer conductance. They coincide for the impurity disorder; however, for the edge roughness they strongly differ, i.e., the diffusive transport in the wire with rough edges is not semiclassical. It becomes semiclassical only for roughness with a large correlation length. The conductance then behaves like the conductance of the wire with impurities, also showing the conductance fluctuations of the same size.

DOI: [10.1103/PhysRevB.83.245328](https://doi.org/10.1103/PhysRevB.83.245328)

PACS number(s): 73.23.–b, 73.20.Fz, 73.61.Ey

I. INTRODUCTION

A wire made of a normal metal is called mesoscopic if the wire length (L) is smaller than the electron coherence length.^{1–3} It is called quasi-one-dimensional (Q1D) if L is much larger than the width (W) and thickness (H) of the wire.³ Fabrication of the Q1D wires from such metals like Au, Ag, Cu, etc., usually involves techniques like electron beam lithography, lift-off, and metal evaporation. These techniques always provide wires with disorder due to the grain boundaries, impurity atoms, and rough wire edges.⁴ Disorder scatters the conduction electrons and limits the electron mean free path (l) in the wires to ~ 10 –100 nm.⁵ Of fundamental interest are the wires with W and H as small as ~ 10 –100 nm.

In this paper the electron transport in metallic Q1D wires is studied theoretically. We compare an impurity-free wire with rough edges with a smooth wire with impurity disorder (a wire with grain boundaries will be studied elsewhere). We study the Q1D wires made of a two-dimensional (2D) conductor ($H \rightarrow 0$) of width W and length $L \gg W$. Our results are representative for wires made of a normal metal as well as of a 2D electron gas at a semiconductor heterointerface.

First we review the basic properties of the Q1D wires. Consider the electron gas confined in the 2D conductor depicted in Fig. 1. At zero temperature, the wave function $\varphi(x, y)$ of the electron at the Fermi level (E_F) is described by the Schrödinger equation,

$$H\varphi(x, y) = E_F\varphi(x, y), \quad (1)$$

with Hamiltonian

$$H = -\frac{\hbar^2}{2m} \left(\frac{\partial^2}{\partial x^2} + \frac{\partial^2}{\partial y^2} \right) + V(x, y) + U_I(x, y), \quad (2)$$

where m is the electron effective mass, $U_I(x, y)$ is the potential due to the impurities, and $V(x, y)$ is the confining potential due to the edges. Following the Fig. 1, the confining potential in a wire with smooth edges can be written as

$$V(y) = \begin{cases} 0, & 0 < y < W \\ \infty, & \text{elsewhere} \end{cases}, \quad (3)$$

while in a wire with rough edges it has to be modified as

$$V(x, y) = \begin{cases} 0, & d(x) < y < h(x) \\ \infty, & \text{elsewhere} \end{cases}, \quad (4)$$

where $d(x)$ and $h(x)$ are the y coordinates of the edges. The potential of the impurities, U_I , is usually assumed to be a white-noise potential.³ The simplest specific choice is

$$U_I(x, y) = \sum_i \gamma \delta(x - x_i) \delta(y - y_i), \quad (5)$$

where one sums over the random impurity positions $[x_i, y_i]$ with a random sign of the impurity strength γ (see Fig. 1). Similar models of disorder as in Fig. 1 are commonly used in the quantum transport simulations.^{6–10}

The disordered Q1D wire is connected to two ballistic semi-infinite contacts of constant width W , as shown in Fig. 2. In the contacts the electrons obey the Schrödinger equation

$$\left[-\frac{\hbar^2}{2m} \left(\frac{\partial^2}{\partial x^2} + \frac{\partial^2}{\partial y^2} \right) + V(y) \right] \varphi(x, y) = E_F \varphi(x, y), \quad (6)$$

where $V(y)$ is the confining potential given by Eq. (3). Solving Eq. (6) one finds the independent solutions

$$\varphi_n^\pm(x, y) = e^{\pm ik_n x} \chi_n(y), \quad n = 1, 2, \dots, \infty, \quad (7)$$

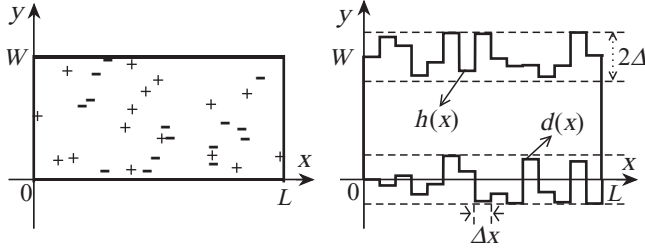


FIG. 1. Wire made of the 2D conductor of width W and length L . The figure on the left depicts the wire with impurities positioned at random with random signs of the impurity potentials. The figure on the right depicts the impurity-free wire with rough edges, where $d(x)$ and $h(x)$ are the y coordinates of the edges at $y = 0$ and $y = W$, respectively, randomly fluctuating with x . The roughness amplitude is Δ and the step Δx also means the correlation length (see the text).

with the wave vectors k_n given by

$$E_F = \epsilon_n + \frac{\hbar^2 k_n^2}{2m}, \quad \epsilon_n \equiv \frac{\hbar^2 \pi^2}{2mW^2} n^2, \quad (8)$$

where ϵ_n is the energy of motion in the y direction and

$$\chi_n(y) = \begin{cases} \sqrt{\frac{2}{W}} \sin\left(\frac{\pi n}{W} y\right), & 0 < y < W \\ 0, & \text{elsewhere} \end{cases} \quad (9)$$

is the wave function in the direction y . The vectors k_n in Eq. (7) are assumed to be positive, i.e., the waves $e^{ik_n x}$ and $e^{-ik_n x}$ describe the free motion in the positive and negative directions of the x axis, respectively. The energy $\epsilon_n + \hbar^2 k_n^2/2m$ is called the n th energy channel. The channels with $\epsilon_n < E_F$ are conducting due to the real values of k_n while the channels with $\epsilon_n > E_F$ are evanescent due to the imaginary k_n . The conducting state $\varphi_n^+(x, y) = e^{ik_n x} \chi_n(y)$ in contact 1 impinges on the disordered wire from the left. It is partly transmitted through disorder and enters contact 2 in the form

$$\varphi_n^+(x, y) = \sum_{m=1}^{\infty} t_{mn} e^{ik_m x} \chi_m(y), \quad x \geq L, \quad (10)$$

where $t_{mn}(k_n)$ is the probability amplitude of transmission from n to m . At zero temperature, the conductance of the disordered wire is given by the Landauer formula¹¹

$$G = \frac{2e^2}{h} \sum_{n=1}^{N_c} T_n = \frac{2e^2}{h} \sum_{n=1}^{N_c} \sum_{m=1}^{N_c} |t_{mn}|^2 \frac{k_m}{k_n}, \quad (11)$$

where we sum over all (N_c) conducting channels. We note that T_n is the transmission probability through disorder for the electron impinging disorder in the n th conducting channel. The amplitudes t_{mn} have to be calculated for specific disorder by solving Eq. (1) with asymptotic condition (10). In the ensemble of macroscopically identical wires, disorder fluctuates from wire to wire and so does the conductance. Hence it is meaningful to evaluate Eq. (11) for the ensemble of wires and to study the ensemble-averaged conductance $\langle G \rangle$, variance $\langle G^2 \rangle - \langle G \rangle^2$, resistance $\langle 1/G \rangle$, etc. We now discuss a few important results of such studies. For simplicity we use the variables $g \equiv G/(2e^2/h)$ and $\rho = 1/g$.

First we discuss the smooth Q1D wires with disorder due to the white-noise potential U_I . For $L = 0$ formula (11) gives the

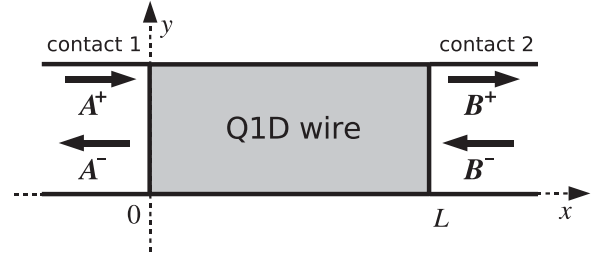


FIG. 2. The Q1D wire placed between two contacts. The bold arrows denote the wave amplitudes A^+ , B^- coming into the wire and the amplitudes A^- , B^+ coming out of the wire.

ballistic conductance $g = N_c$. As L increases, formula (11) first shows the classical transmission law,²

$$\langle g \rangle = N_c \frac{\frac{\pi}{2} l}{(L + \frac{\pi}{2} l)}, \quad 0 < L \ll \xi, \quad (12)$$

where $N_c \gg 1$ and $\xi \simeq N_c l$ is the Q1D localization length. If $l \ll L \ll \xi$, the wire is in the diffusive regime. For $l \ll L$ and $N_c \simeq k_F W/\pi$ we obtain from Eq. (12) the standard expression

$$\langle g \rangle = \sigma_{\text{dif}} W/L, \quad \sigma_{\text{dif}} \equiv \pi n_e l/k_F, \quad l \ll L \ll \xi, \quad (13)$$

where σ_{dif} is the diffusive conductivity, k_F is the 2D Fermi wave vector, and $n_e = k_F^2/2\pi$ is the 2D electron density. However, the mesoscopic diffusive conductance is also affected by weak localization. Hence, one in fact obtains from Eq. (11) a slightly modified version of Eq. (13), namely^{3,12}

$$\langle g \rangle = \sigma_{\text{dif}} W/L - 1/3, \quad l \ll L \ll \xi, \quad (14)$$

where the term $1/3$ is the weak localization correction typical of the Q1D wire. The mean free path l in the above formulas coincides with the mean free path derived from the semiclassical Boltzmann transport equation, i.e., quantum conductance (11) captures the Boltzmann transport limit exactly. The mean of the two-terminal resistance, $\langle \rho \rangle \equiv \langle 1/g \rangle$, shows in absence of weak localization the diffusive behavior²

$$\langle \rho \rangle = \rho_c + \rho_{\text{dif}} L/W, \quad 0 < L \ll \xi, \quad (15)$$

where $\rho_c = 1/N_c$ is the contact resistance and $\rho_{\text{dif}} = 1/\sigma_{\text{dif}}$ is the diffusive resistivity. Diffusive resistance (15) and diffusive conductance (13) thus coexist in a standard way: $\langle \rho \rangle \simeq 1/\langle g \rangle$ for $\rho_{\text{dif}} \frac{L}{W} \gg \rho_c$. If we include the weak localization by means of Eq. (14), then

$$\langle \rho \rangle \simeq 1/\langle g \rangle \simeq \rho_{\text{dif}} \frac{L}{W} + \frac{1}{3} \rho_{\text{dif}}^2 \frac{L^2}{W^2}, \quad l \ll L \ll \xi. \quad (16)$$

The conductance fluctuates in the diffusive regime as^{13,14}

$$\sqrt{\text{var}(g)} \equiv \sqrt{\langle g^2 \rangle - \langle g \rangle^2} = \sqrt{2/15} \simeq 0.365, \quad l \ll L \ll \xi, \quad (17)$$

where the numerical factor 0.365 is typical of the Q1D wire. Finally, as L exceeds ξ , the mesoscopic Q1D wire enters the regime of strong localization, where $\langle g \rangle$ decreases with L exponentially while $\langle \rho \rangle$ shows exponential increase.^{15,16}

Formulas (12)–(17) hold for the wires with impurity disorder. Do they hold also for the wires with rough edges? In this paper we address this question from first principles: We calculate the amplitudes t_{mn} by the scattering-matrix method^{6,7,17} for a large ensemble of macroscopically identical

disordered wires, we evaluate the Landauer conductance (11), and we perform ensemble averaging.

In fact, a few serious differences between the wires with rough edges and wires with impurity disorder were identified prior to our work. In the wire with impurity disorder the channels are equivalent in the sense that $\langle T_1 \rangle = \langle T_2 \rangle \cdots = \langle T_{N_c} \rangle$.^{18,19} For instance, in the diffusive regime $\langle T_n \rangle = \frac{\pi}{2} l/L$ for all channels.² In the impurity-free wires with rough edges, $\langle T_n \rangle$ decays fast with raising n , because the scattering by the rough edges is weakest in the channel $n = 1$ and strongest in the channel $n = N_c$.^{20–24} This is easy to understand classically: In the channel $n = 1$ the electron avoids the edges by moving in parallel with them, while in the channel $n = N_c$ the motion is almost perpendicular to the edges, resulting in frequent collisions with them. As a result, $\langle T_n \rangle$ shows the coexistence of the quasi-ballistic, diffusive, and strongly localized channels.²⁵ Due to this coexistence, the work in this paper reported the absence of the dependence $\langle g \rangle \propto 1/L$, suggesting that the wire with rough edges does not exhibit the diffusive conductance of Eq. (13). However, according to Refs. 21 and 26, the wire with rough edges seems to exhibit the diffusive resistance Eq. (15). In this paper these findings are examined again, but for significantly larger N_c as in previous works.

First we study the impurity-free wire whose edges have a roughness correlation length comparable with the Fermi wavelength. For $L \rightarrow 0$ we observe the quasi-ballistic dependence $1/\langle g \rangle = \langle \rho \rangle = 1/N_c + \rho_{\text{qb}}L/W$, where ρ_{qb} is the quasi-ballistic resistivity. As L increases, we observe crossover to the diffusive dependence $1/\langle g \rangle \simeq \langle \rho \rangle = 1/N_c^{\text{eff}} + \rho_{\text{dif}}L/W$, where $\rho_{\text{dif}} \ll \rho_{\text{qb}}$ and $1/N_c^{\text{eff}}$ is the effective contact resistance due to the N_c^{eff} open channels. We find the universal results $\rho_{\text{qb}}/\rho_{\text{dif}} \simeq 0.6N_c$ and $N_c^{\text{eff}} \simeq 6$ for $N_c \gg 1$. As L exceeds the localization length ξ , the resistance shows the onset of localization while the conductance shows the diffusive dependence $1/\langle g \rangle \simeq 1/N_c^{\text{eff}} + \rho_{\text{dif}}L/W$ up to $L \simeq 2\xi$ and the localization for $L > 2\xi$ only. Finally, we find

$$\sqrt{\text{var}(g)} \equiv \sqrt{\langle g^2 \rangle - \langle g \rangle^2} \simeq 0.3, \quad l \ll L \lesssim 2\xi. \quad (18)$$

The fluctuations in Eq. (18) differ from those in Eq. (17) and were already reported in the past.^{9,25,27,28} For the smooth wires with impurities our calculations confirm formulas (12)–(17).

Moreover, we derive the wire conductivity from the semiclassical Boltzmann equation,^{29–31} and we compare the semiclassical mean free path with the mean free path obtained from the quantum resistivity ρ_{dif} . For the impurity disorder we find that the semiclassical and quantum mean free paths coincide, which is a standard result. However, for the edge roughness the semiclassical mean free path strongly differs from the quantum one, showing that the diffusive transport in the wire with rough edges is not semiclassical. We show that it is semiclassical only if the roughness-correlation length is much larger than the Fermi wavelength. For such edge roughnesses the conductance behaves like the conductance of the wire with impurities [formulas (12)–(17)], also showing the fluctuations of Eq. (17).

The next section describes the scattering-matrix calculation of the amplitudes t_{mn} for the impurity disorder and edge roughness. In Sec. III, the impurity disorder and edge roughness are treated by means of the Boltzmann equation and

the semiclassical Q1D conductivity expressions are derived. In Sec. IV we show our numerical results. Moreover, the crossover from $1/\langle g \rangle = \langle \rho \rangle = 1/N_c + \rho_{\text{qb}}L/W$ to $1/\langle g \rangle \simeq \langle \rho \rangle = 1/N_c^{\text{eff}} + \rho_{\text{dif}}L/W$ in the wire with rough edges is derived by means of a microscopic analytical theory. The theory neglects localization but nevertheless captures the main features of our numerical results. In particular, we obtain analytically the universal results $\rho_{\text{qb}}/\rho_{\text{dif}} = \frac{\pi^3}{24}N_c$ and $N_c^{\text{eff}} \simeq 2.5$. A summary is given in Sec. V.

II. THE SCATTERING-MATRIX APPROACH

Consider the Q1D wire with contacts 1 and 2, shown in Fig. 2. The wave function $\varphi(x, y)$ in the contacts can be expanded in the basis of the eigenstates of Eq. (7). We introduce notations $A_n^\pm(x) \equiv a_n^\pm e^{\pm ik_n x}$ and $B_n^\pm(x) \equiv b_n^\pm e^{\pm ik_n x}$, where a_n^\pm and b_n^\pm are the amplitudes of the waves moving in the positive and negative directions of the x axis, respectively. At the boundary $x = 0$,

$$\varphi(0, y) = \sum_{n=1}^N [A_n^+(0) + A_n^-(0)] \chi_n(y), \quad (19)$$

while at the boundary $x = L$,

$$\varphi(L, y) = \sum_{n=1}^N [B_n^+(L) + B_n^-(L)] \chi_n(y), \quad (20)$$

where N is the considered number of channels (ideally $N = \infty$). We define the vectors $A^\pm(0)$ and $B^\pm(L)$ with components $A_{n=1, \dots, N}^\pm(0)$ and $B_{n=1, \dots, N}^\pm(L)$, respectively, and we simplify the notations $A^\pm(0)$ and $B^\pm(L)$ as A^\pm and B^\pm . The amplitudes A^\pm and B^\pm are related through the matrix equations,

$$\begin{pmatrix} A^- \\ B^+ \end{pmatrix} = \begin{bmatrix} r & t' \\ t & r' \end{bmatrix} \begin{pmatrix} A^+ \\ B^- \end{pmatrix}, \quad S \equiv \begin{bmatrix} r & t' \\ t & r' \end{bmatrix} \quad (21)$$

where S is the scattering matrix. Its dimensions are $2N \times 2N$ and its elements t, r, t' , and r' are the matrices with dimensions $N \times N$. Physically, t and t' are the transmission amplitudes of the waves A^+ and B^- , respectively, while r and r' are the corresponding reflection amplitudes. The matrix elements of the transmission matrix t are just the transmission amplitudes t_{mn} which determine the conductance of Eq. (11).

Consider two wires 1 and 2, described by the scattering matrices S_1 and S_2 . The matrices are defined as

$$S_1 \equiv \begin{bmatrix} r_1 & t'_1 \\ t_1 & r'_1 \end{bmatrix}, \quad S_2 \equiv \begin{bmatrix} r_2 & t'_2 \\ t_2 & r'_2 \end{bmatrix}. \quad (22)$$

Let

$$S_{12} \equiv \begin{bmatrix} r_{12} & t'_{12} \\ t_{12} & r'_{12} \end{bmatrix} \quad (23)$$

be the scattering matrix of the wire obtained by connecting the wires 1 and 2 in series. The matrix S_{12} is related to the matrices S_1 and S_2 through the matrix equations²

$$\begin{aligned} t_{12} &= t_2 [I - r'_1 r_2]^{-1} t_1, \\ r_{12} &= r_1 + t'_1 r_2 [I - r'_1 r_2]^{-1} t_1, \\ t'_{12} &= t'_1 [I + r_2 [I - r'_1 r_2]^{-1} r'_1] t'_2, \\ r'_{12} &= r'_2 + t_2 [I - r'_1 r_2]^{-1} r'_1 t'_2, \end{aligned} \quad (24)$$

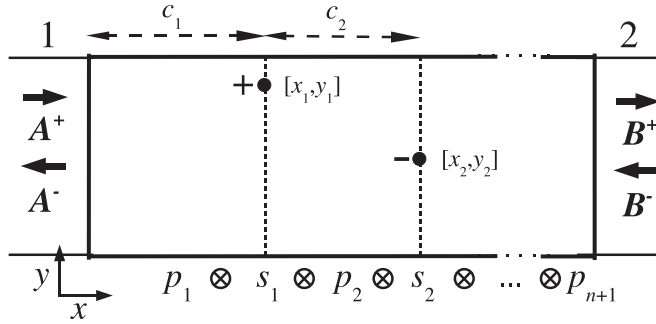


FIG. 3. Wire with the randomly positioned pointlike impurities. The n impurities described by the scattering matrices s_i divide the wire into the $n + 1$ free regions described by the matrices p_i . Also shown are the wave amplitudes A^\pm and B^\pm .

where I is the unit matrix. Equations (24) are usually written in the symbolic form

$$S_{12} = S_1 \otimes S_2. \quad (25)$$

A. Scattering matrix of a smooth wire with impurity disorder

Consider the wire with the impurity potential given in Eq. (5). Between any two neighboring impurities there is a region with zero impurity potential, say the region $x_{i-1} < x < x_i$, where the electron moves along the x axis like a free particle. The wire with n impurities contains $n + 1$ regions with free-electron motion, separated by n pointlike regions where the scattering takes place. As illustrated in Fig. 3, the scattering matrix S of such a wire can be obtained by applying the combination law

$$S = p_1 \otimes s_1 \otimes p_2 \otimes s_2 \otimes \dots \otimes s_n \otimes p_{n+1}, \quad (26)$$

where p_i is the scattering matrix of free motion in the region $x_{i-1} < x < x_i$ and s_i is the scattering matrix of the i th impurity. The symbols \otimes mean that the composition law of Eq. (25) is applied in Eq. (26) step by step: One first combines the matrices p_1 and s_1 , the resulting matrix is combined with p_2 , etc.

The scattering matrix p_i can be expressed as

$$p_i = \begin{bmatrix} 0 & \Phi \\ \Phi & 0 \end{bmatrix}, \quad (27)$$

where 0 is the $N \times N$ matrix with zero matrix elements and Φ is the $N \times N$ matrix with matrix elements

$$\Phi_{mn} = e^{ik_n c_i} \delta_{mn}, \quad c_i = x_i - x_{i-1}, \quad (28)$$

Finally, for a δ -function-like impurity the scattering matrix

$$s_i \equiv \begin{bmatrix} r & t' \\ t & r' \end{bmatrix} \quad (29)$$

is composed of the matrices^{6,7}

$$t = t' = [K + i\Gamma]^{-1} K, \quad (30)$$

$$r = r' = -[K + i\Gamma]^{-1} i\Gamma, \quad (31)$$

where K and Γ are the $N \times N$ matrices with matrix elements

$$K_{mn} = k_n \delta_{mn}, \quad \Gamma_{mn} = \frac{m\gamma}{\hbar^2} \chi_m^*(y_i) \chi_n(y_i). \quad (32)$$

Concerning the value of N , we use $N \geq N_c$ chosen in such a way,⁶ that in the diffusive regime our simulation reproduces the Boltzmann equation results.

B. Scattering matrix of the impurity-free wire with rough edges

The electrons in the impurity-free wire with rough edges are described by Schrödinger Eq. (1) with a Hamiltonian without the impurity potential, but with the confining potential $V(x, y)$ [Eq. (4)], including the edge roughness. We specify the edge roughness as follows. We define $x_j = j\Delta x$, where $j = 0, 1, 2, \dots$, and Δx is a constant step. For x between x_j and x_{j+1} , the smoothly varying functions $V(x, y)$, $h(x)$, and $d(x)$ in Eq. (4) are replaced by constant values $V_j(y) \equiv V(x_j, y)$, $h_j \equiv h(x_j)$, and $d_j \equiv d(x_j)$, respectively. We obtain the equation

$$V_j(y) = \begin{cases} 0, & d_j < y < h_j \\ \infty, & \text{elsewhere} \end{cases}. \quad (33)$$

We assume that d_j and h_j vary with varying j at random in the intervals $(-\Delta, \Delta)$ and $(W - \Delta, W + \Delta)$, respectively. This is depicted in Fig. 1, where $h(x)$ and $d(x)$ fluctuate with varying x by changing abruptly after each step Δx .

The wire width fluctuates with varying x as well. However, for x between x_j and x_{j+1} , we have the constant width

$$W_j = h_j - d_j. \quad (34)$$

Consequently, the electron wave function for x between x_j and x_{j+1} can be expressed in the form

$$\varphi^j(x, y) = \sum_{n=1}^{N_j} [a_n^+ e^{ik_n^j x} + a_n^- e^{-ik_n^j x}] \chi_n^j(y), \quad (35)$$

where N_j is the considered number of channels ($N_j = \infty$ in the ideal case), the wave vectors k_n^j are given by

$$E_F = \epsilon_n^j + \frac{\hbar^2 (k_n^j)^2}{2m}, \quad \epsilon_n^j \equiv \frac{\hbar^2 \pi^2}{2mW_j^2} n^2, \quad (36)$$

$$\chi_n^j(y) = \begin{cases} \sqrt{\frac{2}{W_j}} \sin\left[\frac{\pi n}{W_j}(y - d_j)\right], & d_j < y < h_j \\ 0, & \text{elsewhere} \end{cases} \quad (37)$$

are the wave functions for the y direction, and the index j means that the above equations hold for x between x_j and x_{j+1} . Equations (36) and (37) are just Eqs. (8) and (9), respectively, modified for the wire with rough edges.

In practice we choose N_j by means of the relation¹⁷

$$N^j/N = W_j/W, \quad (38)$$

i.e., the ratio of the channel numbers in the j th region and contact regions is the same as the ratio of their widths. We choose $N \geq N_c$ and we check that the calculated conductance does not depend on the choice of N . For $N \geq N_c$ relation (38) ensures $N^j \geq N_c^j$, where N_c^j is the number of the conducting channels in the j th wire region. This makes the calculation reliable also when N_c^j fluctuates with varying j , which happens for Δ larger than the Fermi wavelength.

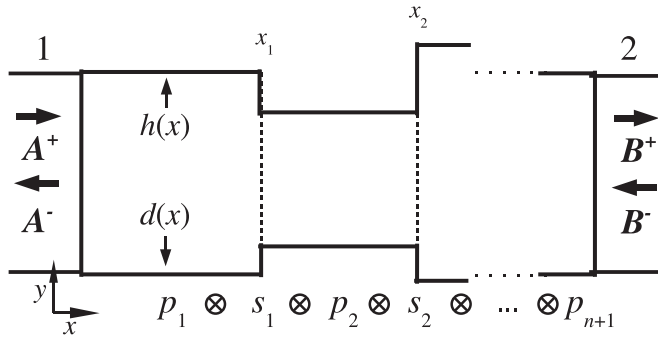


FIG. 4. The impurity-free wire with n edge steps described by the scattering matrices s_j and with $n + 1$ free regions of constant width W_j , described by the scattering matrices p_j .

As shown in Fig. 4, the scattering matrix S of the wire with rough edges is again given by the combination law of Eq. (26), where p_j is the scattering matrix of free motion in the region $x_{j-1} < x < x_j$ and s_j is the scattering matrix of the j th edge step. The scattering matrix p_j is given by Eq. (27) with the matrix elements of Eq. (28) modified as

$$\Phi_{mn} = e^{ik_n^j \Delta x} \delta_{mn}. \quad (39)$$

Finally, we follow Ref. 17 to specify the scattering matrix s_j .

Consider the wire shown in Fig. 5. A single edge step at $x = 0$ divides the wire into region A ($x < 0$) and region B ($x > 0$). The widths of the regions A and B are $W_A = h_A - d_A$ and $W_B = h_B - d_B$, respectively. We consider the case $W_A > W_B$ and we assume that the wire cross-section. W_A includes the wire cross-section. W_B (see the figure). In this situation, the confining potential is simply

$$V(x, y) = \begin{cases} 0, & x < 0, & d_A < y < h_A \\ 0, & x > 0, & d_B < y < h_B. \\ \infty, & \text{elsewhere} \end{cases} \quad (40)$$

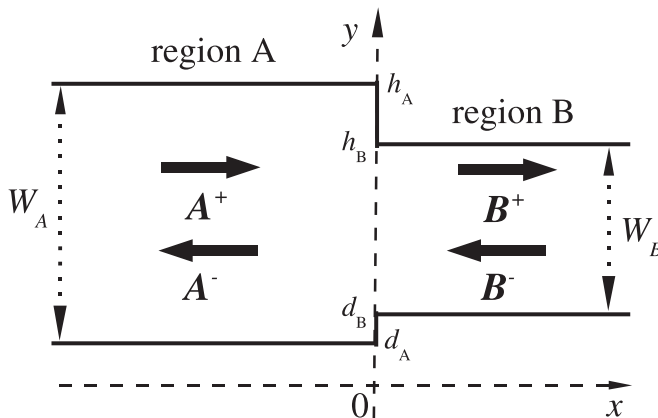


FIG. 5. The wire with a single edge step at $x = 0$. The symbols in the figure are discussed in the text.

So we can use Eq. (35) and write the wave function at $x = 0$ as

$$\varphi(0 - \epsilon, y) = \sum_{n=1}^{N_A} [A_n^+(0) + A_n^-(0)] \chi_n^A(y), \quad \epsilon \rightarrow 0, \quad (41)$$

$$\varphi(0 + \epsilon, y) = \sum_{n=1}^{N_B} [B_n^+(0) + B_n^-(0)] \chi_n^B(y), \quad \epsilon \rightarrow 0, \quad (42)$$

where $A_n^\pm(x) \equiv a_n^\pm e^{\pm ik_n^A x}$, $B_n^\pm(x) \equiv b_n^\pm e^{\pm ik_n^B x}$, and N_A and N_B are the channel numbers in regions A and B. The continuity equation $\varphi(0 - \epsilon, y) = \varphi(0 + \epsilon, y)$ takes the form

$$A^+ + A^- = C(B \rightarrow A)(B^+ + B^-), \quad (43)$$

where $C(B \rightarrow A)$ is the matrix with the matrix elements

$$C(B \rightarrow A)_{mn} = \int_{d_A}^{h_A} \chi_m^{A*}(y) \chi_n^B(y) dy \quad (44)$$

and dimensions $N_A \times N_B$. Similarly, the continuity equation $\frac{\partial \varphi}{\partial x}(0 - \epsilon, y) = \frac{\partial \varphi}{\partial x}(0 + \epsilon, y)$ can be written in the form

$$K^A(A^+ - A^-) = C(B \rightarrow A)K^B(B^+ - B^-), \quad (45)$$

where K^A and K^B are matrices with the matrix elements

$$(K^A)_{mn} = k_n^A \delta_{mn}, \quad (K^B)_{mn} = k_n^B \delta_{mn} \quad (46)$$

and dimensions $N_A \times N_A$ and $N_B \times N_B$, respectively. Combining Eqs. (43) and (45) one finds matrix Eqs. (21) with the scattering matrix $s_j \equiv S$ composed of the matrices

$$\begin{aligned} t &= -2MH_{BA}, \\ r &= -2C(B \rightarrow A)MH_{BA} - I^A, \\ t' &= C(B \rightarrow A)[MN + I^B], \\ r' &= MN, \end{aligned} \quad (47)$$

where

$$\begin{aligned} H_{BA} &= -(K^B)^{-1}C^T(B \rightarrow A)K^A, \\ M &= [I^B - H_{BA}C(B \rightarrow A)]^{-1}, \\ N &= I^B + H_{BA}C(B \rightarrow A), \end{aligned} \quad (48)$$

with I^A and I^B being the unit matrices and C^T being the matrix obtained by transposition of the matrix C . The dimensions of the matrices t , r , t' , and r' are $N_B \times N_A$, $N_A \times N_A$, $N_A \times N_B$, and $N_B \times N_B$, respectively.

Proceeding in a similar way one can derive s_j for the situation $W_A < W_B$, with the cross-section. W_A included in the cross section. W_B . In this case s_j is composed of the matrices

$$\begin{aligned} t &= C(A \rightarrow B)[MN + I^A], \\ r &= MN, \\ t' &= -2MH_{AB}, \\ r' &= -2C(A \rightarrow B)MH_{AB} - I^B, \end{aligned} \quad (49)$$

where M , H_{AB} , and N are the matrices of Eq. (48) with the index A replaced by B and vice versa.

C. Averaging over the samples made of the building blocks

The conductance of Eq. (11) needs to be evaluated for a large ensemble of macroscopically identical wires because it fluctuates from wire to wire. To evaluate the ensemble-averaged results like $\langle g \rangle$, $\langle g^2 \rangle - \langle g \rangle^2$, $\langle 1/g \rangle$, etc., we need to perform averaging typically over $10^3 - 10^4$ samples with different microscopic configurations of disorder. Moreover, the ensemble averages are studied as depending on the wire length. Especially for long wires ($L \sim \xi$) with a large number of conducting channels ($N_c \sim 30 - 300$) already the scattering-matrix calculation of a single disordered sample takes a lot of computational time. To decrease the total computational time substantially (say by a few orders of magnitude), we introduce a few efficient tricks, partly motivated by Ref. 32.

We recall that two scattering matrices, S_1 and S_2 , can be combined by means of the operation of Eqs. (24), written symbolically as $S_1 \otimes S_2$. This operation is associative, i.e.,

$$(S_1 \otimes S_2) \otimes S_3 = S_1 \otimes (S_2 \otimes S_3). \quad (50)$$

The property of Eq. (50) allows us to proceed as follows. We can construct the disordered wire of length L by joining a large number of short wires (building blocks), where each block has the same length (L_b) and contains the same number (n_b) of scatterers (impurities or edge steps). The scattering matrix of such wire can be expressed as

$$S = b_1 \otimes b_2 \otimes \dots = (p_1 \otimes s_1 \otimes \dots \otimes s_{n_b}) \otimes (p_{n_b+1} \otimes s_{n_b+1} \otimes \dots \otimes s_{2n_b}) \otimes \dots, \quad (51)$$

where $b_1 = p_1 \otimes s_1 \otimes \dots \otimes s_{n_b}$ is the scattering matrix of the first block, $b_2 = p_{n_b+1} \otimes s_{n_b+1} \otimes \dots \otimes s_{2n_b}$ is the scattering matrix of the second block, etc. In the simulation, we can create the N_b different blocks (typically $N_b = 100$) so that we select at random the positions of the n_b scatterers in a given block. Then we evaluate the scattering matrices (b_i) of all N_b blocks. We can now readily study the wire lengths $L = L_b, 2L_b, 3L_b, \dots$, by applying one of the two approaches described below.

A single sample of length $L = jL_b$ can be constructed by joining j blocks, where each block is chosen at random from the N_b blocks. Clearly, one can in principle construct $(N_b)^j$ different samples of length jL_b , but in practice a much smaller number of samples ($\sim 10^3 - 10^4$) is sufficient. The S matrix of each sample can be evaluated by means of Eq. (51) and ensemble averaging can be performed. Already this approach works much faster than the approach which combines in each sample the S matrices of all individual scatterers. A further significant improvement is achieved as follows.

As before, we evaluate the scattering matrices b_i for all N_b blocks, but we apply a more sophisticated algorithm: (i) We choose at random a single b_i matrix describing a specific sample of length $L = L_b$. (ii) Choosing at random another b_i and combining it with the previous one by means of Eq. (51) we obtain the S matrix of a specific sample of length $L = 2L_b$. (iii) Choosing at random another b_i and combining it with the S matrix obtained in the preceding step, we obtain the S -matrix of a specific sample of length $L = 3L_b$. In this way we obtain a set of the Landauer conductances $\{G(jL_b)\}_{j=1,2,\dots}$ for a set of the specific samples with lengths $L = L_b, 2L_b, \dots$. Repeating the algorithm again we obtain a new set $\{G(jL_b)\}_{j=1,2,\dots}$.

Repeating the algorithm say 10^3 times we obtain 10^3 various sets of $\{G(jL_b)\}_{j=1,2,\dots}$, and we perform ensemble averaging separately for each j . This approach saves a lot of time because the S matrix of the sample of length $L = jL_b$ is created by combining a single b_i matrix with the S matrix of a sample of length $L = (j-1)L_b$.

In reality the positions of all scatterers differ from sample to sample. If we take this into account in our simulation, the ensemble-averaged results are the same (within statistical noise) as those obtained by means of our trick, but the ensemble averaging takes far much more computational time. Owing to our trick we can analyze much larger systems, which is essential for a successful observation of our major results.

III. SEMICLASSICAL CONDUCTIVITY OF THE Q1D WIRE

In this section, the semiclassical Q1D conductivity expressions are derived both for the impurity disorder and edge roughness. Precisely, we assume that the electron motion is semiclassical along the direction parallel with the wire and quantized in the perpendicular direction. Our approach is technically similar to the previous studies of the Q1D wires^{31,33} and quantum 2D (Q2D) slabs.^{29,30,34,35}

The semiclassical conductivity of the Q1D wire is given as

$$\sigma = \frac{2}{FW} \sum_n \sum_k \left(-\frac{e}{L}\right) \frac{\hbar k}{m} f_n(k), \quad (52)$$

where F is the electric field applied along the wire, $f_n(k)$ is the electron distribution function in the n th conducting channel, and the factor of 2 includes two spin orientations. Similar to the usual textbook approach, we express $f_n(k)$ as

$$f_n(k) = f(E_{nk}) + \frac{eF}{\hbar} \frac{\partial f(E_{nk})}{\partial k} \tau_n(E_{nk}), \quad (53)$$

where $f(E_{nk}) = 1/(\exp[(E_{nk} - E_F)/k_B T] + 1)$ is the equilibrium occupation number of the electron state with energy $E_{nk} = \epsilon_n + \hbar^2 k^2/2m$ and $\tau_n(E_{nk})$ is the relaxation time. Setting Eq. (53) into Eq. (52) we obtain at zero temperature

$$\sigma = \frac{2e^2}{\pi m W} \sum_{n=1}^{N_c} k_n \tau_n(E_F), \quad (54)$$

where k_n is the Fermi wave vector in the channel n [Eqs. (8)]. Function (53) obeys the linearized Boltzmann equation,

$$-\frac{eF}{\hbar} \frac{\partial f(E_{nk})}{\partial k} = \sum_{n'} \sum_{k'} W_{n,n'}(k,k') [f_{n'}(k') - f_n(k)], \quad (55)$$

where

$$W_{n,n'}(k,k') = \frac{2\pi}{\hbar} |\langle n', k' | U | n, k \rangle|_{\text{av}}^2 \delta(E_{nk} - E_{n'k'}) \quad (56)$$

is the Fermi-golden-rule probability of scattering from $|n, k\rangle$ to $|n', k'\rangle$, with U being the scattering-perturbation potential and $|n, k\rangle = L^{-1/2} \exp(ikx) \chi_n(y)$ being the unperturbed electron state. The index av means that $W_{n,n'}(k,k')$ is averaged over different configurations of disorder.

From Eq. (55) we find (see Appendix A) the relaxation time

$$\tau_n(E_F) = \frac{m}{2\pi^2 \hbar} \sum_{n'} (K^{-1})_{nn'} k_{n'}, \quad (57)$$

where K is the matrix with matrix elements

$$K_{nn'} = \frac{1}{L} \sum_k \sum_{k'} \left[\delta_{nn'} \sum_{\mu} |\langle n, k | U | \mu, k' \rangle|_{\text{av}}^2 \times k^2 \delta(E_{nk} - E_F) \delta(E_{\mu k'} - E_F) - |\langle n, k | U | n', k' \rangle|_{\text{av}}^2 \times k k' \delta(E_{nk} - E_F) \delta(E_{n'k'} - E_F) \right]. \quad (58)$$

The Boltzmann Q1D conductivity thus reads

$$\sigma = \frac{2e^2}{h} \frac{1}{\pi^2 W} \sum_{n=1}^{N_c} \sum_{n'=1}^{N_c} k_n k_{n'} (K^{-1})_{nn'}. \quad (59)$$

A. Semiclassical conductivity of the Q1D wire with impurities

If we set for U the impurity potential of Eq. (5), the matrix elements of Eq. (58) can be expressed (see Appendix B) in the form

$$K_{nn'} = \frac{n_I \bar{\gamma}^2}{\pi^2 W} \left(\frac{1}{2} + \sum_{\mu=1}^{N_c} \frac{k_n}{k_{\mu}} \right) \delta_{nn'}, \quad (60)$$

where

$$\bar{\gamma} = m\gamma/\hbar^2. \quad (61)$$

Using Eq. (60) we obtain from Eq. (59) the Q1D conductivity

$$\sigma = \frac{2e^2}{h} \frac{1}{\bar{\gamma}^2 n_I} \sum_{n=1}^{N_c} \frac{k_n^2}{\frac{1}{2} + \sum_{n'=1}^{N_c} \frac{k_n}{k_{n'}}}. \quad (62)$$

For $N_c \gg 1$ the sum in Eq. (62) converges to $k_F^2/2$, and Eq. (62) converges to the 2D limit

$$\sigma = \frac{2e^2}{h} \frac{k_F}{2} \frac{k_F}{\bar{\gamma}^2 n_I}, \quad (63)$$

derivable from the 2D Boltzmann equation.

B. Semiclassical conductivity of the Q1D wire with rough edges

To evaluate the conductivity of Eq. (59) for the wire with rough edges, we need to determine the perturbation potential U produced by the edge roughness potential in Fig. 1 to set the resulting U into the right-hand side of Eq. (58), and to evaluate $K_{nn'}$. All this is performed in Appendix C. The result is

$$K_{nn'} = \frac{\pi^2 \delta^2}{W^6} \left[\delta_{nn'} \sum_{\mu}^{N_c} n^2 \mu^2 \frac{k_n}{k_{\mu}} [\mathcal{F}(|k_{\mu} - k_n|) + \mathcal{F}(|k_{\mu} + k_n|)] - n^2 n'^2 [\mathcal{F}(|k_n - k_{n'}|) - \mathcal{F}(|k_n + k_{n'}|)] \right], \quad (64)$$

where δ is the root mean square of the fluctuations of the edge coordinates $d(x)$ and $h(x)$ (see below) and $\mathcal{F}(q)$ is the Fourier transform of the roughness correlation function $F(x)$.

To specify δ , $F(x)$, and $\mathcal{F}(q)$ we recall (see Fig. 1) that $d(x)$ and $h(x)$ fluctuate with varying x in the intervals $(-\Delta, \Delta)$ and $(W - \Delta, W + \Delta)$, respectively, by changing their values

abruptly after constant steps Δx . Obviously, the values of $d(x)$ are distributed in the interval $(-\Delta, \Delta)$ with the box-shaped distribution. Using such a distribution we find, that

$$\langle d(x)^2 \rangle - \langle d(x) \rangle^2 = \langle d(x)^2 \rangle = \Delta^2/3 \equiv \delta^2, \quad (65)$$

where the symbol δ labels the root mean square of $d(x)$. The correlation function $F(x)$ is defined as

$$\langle d(x_1 + x)d(x_1) \rangle = \delta^2 F(x). \quad (66)$$

We use the box distribution and we take into account that the step Δx plays the role of the correlation length. We obtain

$$F(x) = \begin{cases} 1 - |x|/\Delta x, & |x| \leq \Delta x \\ 0, & |x| > \Delta x \end{cases}. \quad (67)$$

The Fourier transform of the last equation is

$$\mathcal{F}(q) = \Delta x \frac{2(1 - \cos(\Delta x q))}{(\Delta x q)^2}. \quad (68)$$

The same results as for $d(x)$ hold also for $h(x) - W$, because the roughness of both edges is the same.

IV. NUMERICAL AND ANALYTICAL RESULTS

In Sec. IV A, the quantum transport in the wires with impurity disorder and wires with rough edges is simulated in the quasi-ballistic, diffusive, and localized regimes. In Sec. IV B the crossover from the quasi-ballistic to diffusive regime is explained by means of an intuitive model based on the concept of the open channels. A microscopic analytical theory of the crossover is given in Sec. IV C. In Sec. IV D, the diffusive mean free path obtained from the Landauer conductance and mean free path from the Boltzmann theory are compared for both types of disorder. In Sec. IV E the wire with rough edges is studied for large roughness-correlation lengths.

In principle, all our transport results can be expressed and presented in dependence on the dimensionless variables, Δ/λ_F , $\Delta x/\lambda_F$, W/λ_F , etc., with the Fermi wave length λ_F being the length unit. Nevertheless, in a few cases we also use the normal (not dimensionless) variables, and we present the results for the material parameters $m = 9.109 \times 10^{-31}$ kg and $E_F = 5.6$ eV ($\lambda_F = 0.52$ nm), typical of the Au wires.

A. Quantum transport in wires with impurities and rough edges

We mostly simulate the wires with the number of the conducting channels being $N_c = 34$. This number emulates the limit $N_c \gg 1$ without spending too much computational time. Whenever needed, we also use much larger N_c , the largest one being $N_c = 347$. We calculate the Landauer conductance for 10^4 wires and we evaluate the means.

We start with discussion of the mean resistance $\langle \rho \rangle$. In Fig. 6 the mean resistance of the wire with impurity disorder is compared with the mean resistance of the wire with rough edges for various parameters of disorder. The data obtained for various parameters tend to collapse to a single curve when plotted depending on the ratio L/l . Hence it is sufficient to discuss only the data for one specific choice of parameters.

Figure 7 shows the selected numerical data (solid lines) from Fig. 6. In accord with the textbooks,¹⁻³ the mean

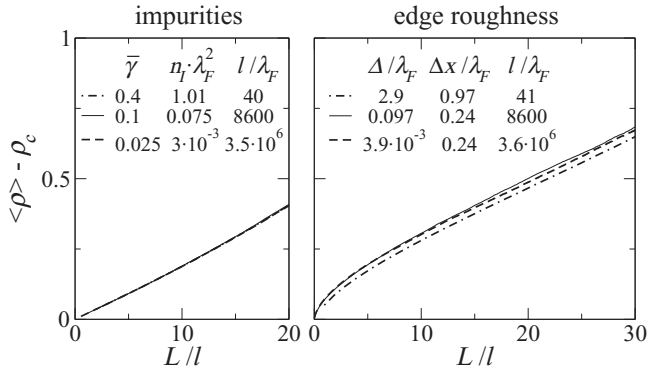


FIG. 6. The mean resistance $\langle \rho \rangle$ as a function of the wire length L . Note that $\langle \rho \rangle$ is reduced by the contact resistance $\rho_c = 1/N_c$ and L is scaled by the mean free path l . The left panel shows the mean resistance of the wire with impurity disorder; the right one shows the mean resistance of the wire with rough edges. The wire width W is fixed to the value $W/\lambda_F = 17.4$, which means that $N_c = 34$. The parameters of disorder are listed in the figure together with the resulting values of l . Determination of l is demonstrated in the next figure. Note that for the Au wire ($E_F = 5.6$ eV and $m = 9.109 \times 10^{-31}$ kg) we have $\lambda_F = 0.52$ nm and $W = 17.3\lambda_F = 9$ nm, with the smallest Δ being only 0.01 nm. Such small Δ is obviously not realistic, but it is used to emulate the weak roughness limit.

resistance of the wire with impurities follows for $L \geq 0$ the standard diffusive dependence $\langle \rho \rangle = \rho_c + \rho_{\text{dif}}L/W$. However, the mean resistance of the wire with rough edges shows a more complex behavior. For $L \rightarrow 0$ it follows the linear dependence $\langle \rho \rangle = \rho_c + \rho_{\text{qb}}L/W$, where ρ_{qb} is the quasi-ballistic resistivity. Only for large-enough L does, it shows crossover to the diffusive dependence $\langle \rho \rangle = \rho_c^{\text{eff}} + \rho_{\text{dif}}L/W$, where the resistivity ρ_{dif} is much smaller than ρ_{qb} and the

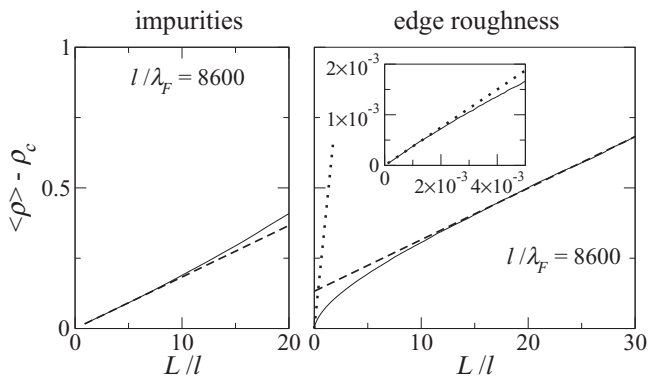


FIG. 7. The solid lines show the selected numerical data from the preceding figure. The dashed line in the left panel shows the linear fit $\langle \rho \rangle = \rho_c + \rho_{\text{dif}}L/W$, while the dashed line in the right panel is the linear fit $\langle \rho \rangle = \rho_c^{\text{eff}} + \rho_{\text{dif}}L/W$, with ρ_c^{eff} being the effective contact resistance. In both cases the resistivity ρ_{dif} is a fitting parameter and l is extracted from the Drude formula $\rho_{\text{dif}} = 2/(k_F l)$. To determine ρ_c^{eff} , the dashed line in the right panel is extrapolated to $L = 0$. We find $\rho_c^{\text{eff}} \simeq 1/7.5$ while $\rho_c = 1/34$, the inset shows the solid line from the right panel for $L/l \ll 1$, where the transport is quasi-ballistic. The dotted lines show the linear fit $\langle \rho \rangle = \rho_c + \rho_{\text{qb}}L/W$, where the quasi-ballistic resistivity ρ_{qb} is a fitting parameter. The quasi-ballistic mean free path l_{qb} is given as $l_{\text{qb}} = 2/(k_F \rho_{\text{qb}})$.

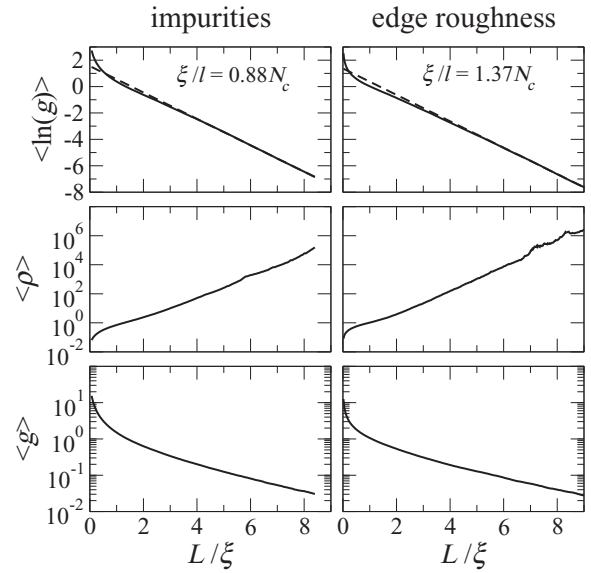


FIG. 8. Typical conductance $\langle \ln g \rangle$, mean resistance $\langle \rho \rangle$, and mean conductance $\langle g \rangle$ versus L/ξ . The results for the wire with impurity disorder (left panels) are compared with the results for the wire with rough edges (right panels). The calculations were performed for various sets of the parameters, listed in the Fig. 6. The results for various parameter sets collapse to a single curve shown as a solid line (see the remarks in the text). The dashed lines in the top panels show the fit $\langle \ln g \rangle = -L/\xi$, from which we determine the localization length ξ . The resulting values of ξ are shown.

effective contact resistance ρ_c^{eff} strongly exceeds the fundamental contact resistance ρ_c . In other words, the wire with rough edges shows two different linear regimes (the quasi-ballistic one and the diffusive one) separated by crossover, while the wire with impurities shows a single linear regime for the quasi-ballistic as well as diffusive transport.

Figure 7 also shows that the mean resistance of the wire with impurities increases for $L/l \gtrsim 10$ slightly faster than linearly, which is due to the weak localization. However, the mean resistance of the wire with rough edges increases linearly even for $10 \lesssim L/l \lesssim 30$. The origin of this difference will become clear soon.

Figure 8 shows the numerical results (solid lines) for the typical conductance $\langle \ln g \rangle$, mean resistance $\langle \rho \rangle$, and mean conductance $\langle g \rangle$ depending on the ratio L/ξ . The calculations were performed for various sets of the parameters, shown in Fig. 6. The results for various sets tend to collapse to a single curve (solid line) when plotted as depending on L/ξ . We see for both types of disorder that the numerical data for $\langle \ln g \rangle$ approach at large L the dependence $\langle \ln g \rangle = -L/\xi$. This is a sign of the localization.^{14,36} Fitting of the numerical data provides the values of ξ shown in the figure. In the wire with impurities we find the result $\xi/l \simeq 0.9N_c$, which agrees with the theoretical³⁷ prediction $\xi/l = N_c$ and with numerical studies.⁶ In the wire with rough edges we find $\xi/l \simeq 1.4N_c$. This does not contradict the work,^{21,26} which reports $\xi/l_{1D} \simeq N_c$, but l_{1D} is $\pi/2$ times larger than our l . Finally, due to the localization, $\langle \rho \rangle$ and $\langle g \rangle$ also depend on L/ξ exponentially at large L/ξ .

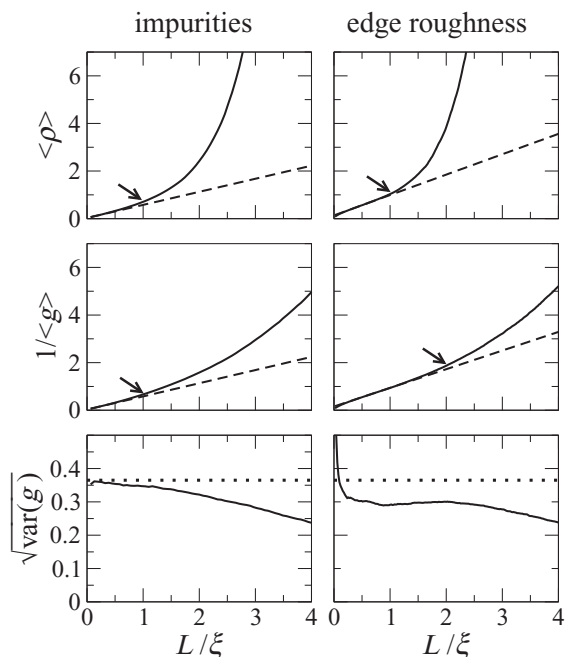


FIG. 9. The solid lines show our numerical data for the mean resistance $\langle \rho \rangle$, inverse mean conductance $1/\langle g \rangle$, and conductance fluctuations $\sqrt{\text{var}(g)}$. The dashed lines in the top panels are the linear fits $\langle \rho \rangle = \rho_c + \rho_{\text{dif}} L/W$ (left panel) and $\langle \rho \rangle = \rho_c^{\text{eff}} + \rho_{\text{dif}} L/W$ (right panel). The dashed lines in the middle panels are the linear fits $1/\langle g \rangle = \rho_c + \rho_{\text{dif}} L/W$ (left panel) and $1/\langle g \rangle = \rho_c^{\text{eff}} + \rho_{\text{dif}} L/W$ (right panel). Onset of strong localization is marked by arrows at the points, where the numerical data start to deviate from the linear fit remarkably. The relative deviation from the linear fit is shown in a separate figure [Fig. (10)]. The dotted line in the bottom panels shows the theoretical value (0.365) of the conductance fluctuations, predicted in the limit $l/\xi \ll L/\xi \ll 1$ for the white-noise disorder.

Figure 9 show the mean resistance $\langle \rho \rangle$ and inverse mean conductance $1/\langle g \rangle$, now in the linear scale. Concerning the mean resistance, the wire with rough edges and wire with impurities behave similarly: $\langle \rho \rangle$ rises with L/ξ linearly on the scale $l/\xi \ll L/\xi \lesssim 1$, as is typical for the diffusive regime. However, both types of wires show a quite different $1/\langle g \rangle$. In the wire with impurities, $1/\langle g \rangle$ rises with L/ξ linearly in the interval $l/\xi \ll L/\xi \lesssim 1$, while in the wire with rough edges $1/\langle g \rangle$ shows the linear rise with L/ξ in the interval as large as $l/\xi \ll L/\xi \lesssim 2$. The $\langle g \rangle \propto 1/L$ dependence is a sign of the diffusive conductance regime, which now persists up to $L/\xi \simeq 2$ and which was not observed in Ref. 20 due to the too narrow length window (as explained by the authors).

Further, the slope of the dashed lines is larger for the edge roughness than for the impurities. This can be understood if we write the Eq. $\langle \rho \rangle \simeq 1/\langle g \rangle \simeq (2/\pi)(\xi/N_c l)(L/\xi)$ and we realize that the ratio $\xi/N_c l$ is larger for the edge roughness.

Figure 9 also shows the conductance fluctuations. The fluctuations in the wire with impurities approach the universal value 0.365, derived^{13,14} in the limit $l/\xi \ll L/\xi \ll 1$ for the white-noise disorder. It is remarkable that the fluctuations in the wire with rough edges show a length-independent universal value (of size ~ 0.3) just in the interval $l/\xi \ll L/\xi \lesssim 2$, in which we see the linear rise of $1/\langle g \rangle$. Coexistence of

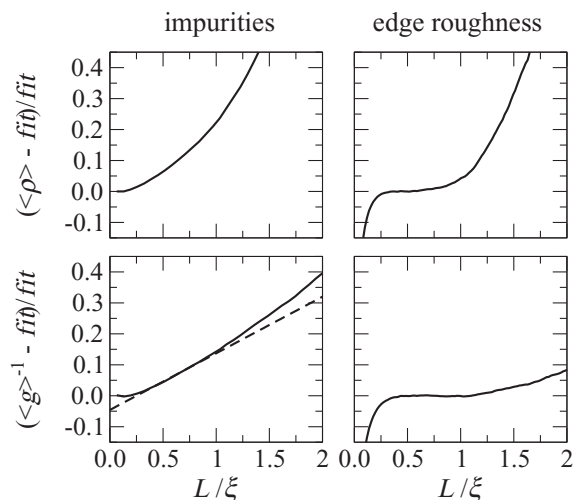


FIG. 10. Numerical data for $\langle \rho \rangle$ and $1/\langle g \rangle$ from the preceding figure, presented as a relative deviation from the linear fit. The dashed line shows the weak-localization-mediated relative deviation $\frac{1}{3}\rho_{\text{dif}}\frac{L}{W}$, shifted by replacement $L \rightarrow (L - 8l)$ to obey the limit $L \gg l$.

the universal conductance fluctuations with the conductance $\sim \xi/L$ is typical of the diffusive conductance regime.²

In Fig. 9, onset of strong localization is visible on first glance at the points (marked by arrows), where the numerical data for $\langle \rho \rangle$ and $1/\langle g \rangle$ start to deviate from the linear dependence remarkably. For the edge roughness the inverse conductance shows onset of localization at $L \simeq 2\xi$: Note that the corresponding conductance fluctuations are not universal just for $L > 2\xi$ (they decay with L).

Figure 10 shows the relative deviation from the linear fit, obtained from the numerical data in Fig. 9. Also shown is the relative deviation $\frac{1}{3}\rho_{\text{dif}}\frac{L}{W}$, obtained from formula (16). As expected, the inverse conductance of the wire with impurities exhibits for $l \ll L < \xi$ the deviation close to $\frac{1}{3}\rho_{\text{dif}}\frac{L}{W}$. This is evidently not the case for the wire with rough edges. First, if $L \lesssim 0.2\xi$, both $\langle \rho \rangle$ and $1/\langle g \rangle$ show a large negative deviation due to the crossover from the quasi-ballistic to diffusive regime. Second, if $0.2\xi \leq L \leq 2\xi$, then $1/\langle g \rangle$ shows a deviation as small as $\lesssim 0.08$ and almost no deviation for $0.4\xi \lesssim L \lesssim 1.1\xi$. In other words, $1/\langle g \rangle$ exhibits up to $L \simeq 2\xi$ the linear diffusive behavior with a minor nonlinear deviation. Finally, $\langle \rho \rangle$ shows a steeply increasing deviation at $L \simeq \xi$ due to the localization.

We have so far discussed the numerical data for the wire parameters listed in Fig. 6. Apart from small differences due to the statistical noise, these data collapse almost precisely to the same curve, when plotted as depending on L/ξ . In fact, such single-parameter scaling (with a dependence solely on L/ξ) holds exactly for weak disorder.^{19,38,39} If disorder is not weak, the data can deviate from the single-parameter scaling and the question is whether our findings hold generally.

For instance, already in Fig. 6 we do not see for various parameters exactly the same curves. However, the difference between various curves is so small that the findings extracted from one of these curves (see Fig. 7) are obtainable with a minor quantitative change from other curves. So we expect

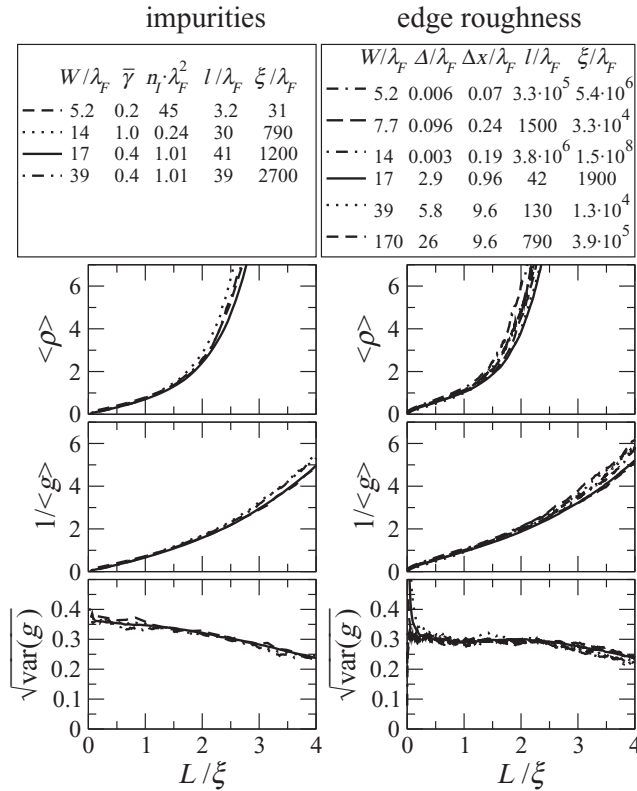


FIG. 11. Mean resistance $\langle \rho \rangle$, inverse mean conductance $1/\langle g \rangle$, and conductance fluctuations $\sqrt{\text{var}(g)}$ for various wire parameters.

that the same findings hold for any (reasonable) choice of the wire parameters. A strong support for this expectation is that the parameters used in Fig. 6 are very different: The mean free paths l range from $l/\lambda_F = 41$ up to $l/\lambda_F = 3.6 \times 10^6$.

Figure 11 shows again the numerical data for $\langle \rho \rangle$, $1/\langle g \rangle$, and $\sqrt{\text{var}(g)}$, but for various sets of the wire parameters. Obviously, the data for various sets do not collapse exactly to the same curve. This may be due to the fact that disorder is not weak; however, the resulting curves are also sensitive to how accurately we determine ξ . We could improve proximity of the curves in Fig. 11 by simulating a larger ensemble of samples and a larger wire length (in order to obtain a more accurate ξ). However, the presented proximity is quite sufficient in the sense that each of the curves allows us to obtain the results very similar to those in Figs. 9 and 10. Proximity of the curves is satisfactory also with regards to the fact that the values of ξ obtained for various parameters in Fig. 11 vary in the range of five orders of magnitude. In this respect we can also say that Fig. 11 confirms universality of the conductance fluctuations in the wire with rough edges: they are of size $\sqrt{\text{var}(g)} \simeq 0.3$, as reported by others.^{9,25,27,28}

B. Crossover from the quasi-ballistic to diffusive transport in wires with rough edges: Intuitive analytical derivation

Let us examine the crossover from $\langle \rho \rangle = \rho_c + \rho_{\text{qb}}L/W$ to $\langle \rho \rangle = \rho_c^{\text{eff}} + \rho_{\text{dif}}L/W$, observed in Fig. 7. Such crossover was not observed in Refs. 21 and 26 where a similar situation was studied numerically. Therefore, we first analyze the conditions

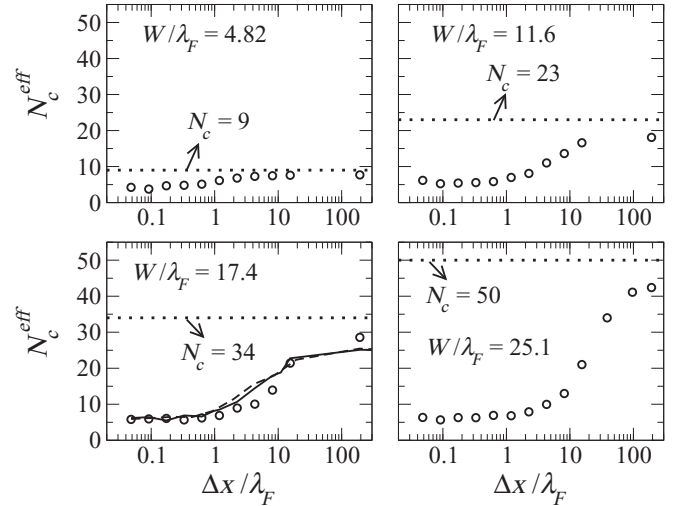


FIG. 12. Effective number of open channels, N_c^{eff} , versus the roughness correlation length Δx for various N_c and various roughness amplitudes Δ . The parameters of the edge roughness are scaled as $\Delta x/\lambda_F$ and Δ/W . The results for $\Delta/W = 1/18$ are shown by open circles; the dashed and solid lines show the results for $\Delta/W = 1/180$ and $\Delta/W = 1/900$, respectively.

of observability. We define the effective number of the open channels, $N_c^{\text{eff}} = 1/\rho_c^{\text{eff}}$, and we evaluate N_c^{eff} numerically (by means of the same procedure as in Fig. 7).

Figure 12 shows N_c^{eff} as depending on the roughness-correlation length Δx for various N_c and various Δ . We see that N_c^{eff} reaches for $\Delta x/\lambda_F \rightarrow 0$ a minimum value which is roughly 6 and which depends, within our numerical accuracy, on neither N_c nor Δ/W . In other words, N_c^{eff} approaches for $\Delta x \rightarrow 0$ the universal value ~ 6 . The calculations in Refs. 21 and 26 were performed for $\Delta x \simeq 0.5\lambda_F$, but only for $N_c = 5$. This value is obviously too small for noticing the existence of $N_c^{\text{eff}} \sim 6$. Hence the Refs. 21 and 26 reported the diffusive dependence $\langle 1/g \rangle \simeq 1/N_c + \rho_{\text{dif}}L/W$ rather than the dependence $\langle 1/g \rangle \simeq 1/N_c^{\text{eff}} + \rho_{\text{dif}}L/W$. Finally, for $\Delta x/\lambda_F \gg 1$ we see that N_c^{eff} approaches N_c . That limit is studied in the Sec. IV E.

Further, we look at the numerical data for $\langle T_n \rangle$, shown in Fig. 13. The theory based on the white-noise disorder predicts that the conducting channels are equivalent^{18,19} in the sense that $\langle T_1 \rangle = \langle T_2 \rangle \cdots = \langle T_{N_c} \rangle$. In Fig. 13, this equivalency is reasonably confirmed for the wire with impurity disorder but not for the wire with rough edges. In the wire with rough edges, $\langle T_n \rangle$ decays fast with raising n which is easy to understand classically: In the channel $n = 1$ the electron avoids the edges by moving in parallel with them, while in the channel $n = N_c$ the motion is almost perpendicular to the edges, resulting in frequent collisions with them. As a result, the $\langle T_n \rangle$ dependence in the right panels of Fig. 13 shows for $L \simeq \xi$ the coexistence of the quasi-ballistic, diffusive, and strongly localized channels, already reported in previous works.^{8,20,25}

Concerning the coexistence, two comments are needed. Evidently, the coexistence is not in contradiction to the fact that all T_n decay in semilogarithmic scale linearly with a single parameter L/ξ , when $L \gg \xi$ (see also Ref. 8). Further, it is

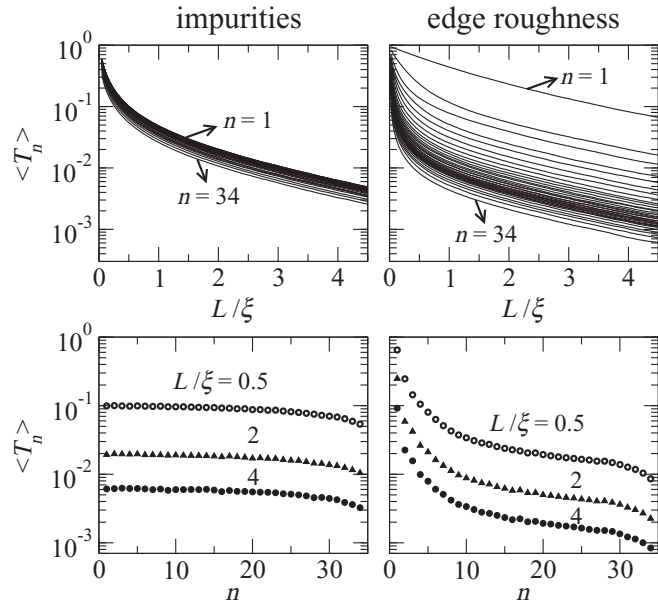


FIG. 13. The top panels show the transmission probability $\langle T_n \rangle$ versus L/ξ for the channel indices $n = 1, 2, \dots, N_c$, where $N_c = 34$. For n ordered increasingly, the resulting curves are ordered decreasingly: The top curve shows $\langle T_{n=1} \rangle$, the bottom one shows $\langle T_{n=N_c} \rangle$. The bottom panels show $\langle T_n \rangle$ versus n for various L/ξ .

clear that if the diffusive regime means $T_n \propto 1/L$ in all N_c channels at the same value of L , then there is no diffusive regime but only crossover from the quasi-ballistic regime to the localization regime.²⁰ In the preceding text we were speaking about the diffusive regime in the sense^{21,26} that $\langle \rho \rangle \propto L$ and $1/\langle g \rangle \propto L$.

For the uncorrelated impurity disorder, the transmission $\langle T_n \rangle$ in the absence of the wave interference takes the form²

$$\langle T_n \rangle = L_n / (L_n + L), \quad (69)$$

where L_n is the characteristic length. For the edge roughness we can adopt Eq. (69) as an ansatz. We will prove later that the ansatz is indeed correct for the uncorrelated roughness. In what follows we combine ansatz (69) with the concept of open channels, and we explain all major features of the crossover from the quasi-ballistic regime to the diffusive one, albeit formula (69) cannot capture the fact that besides the quasi-ballistic and diffusive channels there are also the localized ones.

We assess L_n from the numerical data in Fig. 13. From Fig. 13 it is obvious that L_n in the channels with $n \gg 1$ is much smaller than L_n in the channels with $n \rightarrow 1$. We emulate these findings by a simple model. We introduce the number $N_c^{\text{eff}} \ll N_c$ and we assume that the channels $n = 1, 2, \dots, N_c^{\text{eff}}$ have the characteristic length L_a , while the rest of the channels have the characteristic length $L_b \ll L_a$.

By means of the above model, we can estimate the mean resistance $\langle \rho \rangle$ and mean conductance $\langle g \rangle$ for the wire lengths $0 \leq L \lesssim \xi$. From Fig. 9 we see that

$$\langle \rho \rangle \simeq 1/\langle g \rangle, \quad 0 \leq L \lesssim \xi. \quad (70)$$

We therefore rely on the equation

$$\langle \rho \rangle \simeq \frac{1}{\langle g \rangle} = \frac{1}{\sum_{n=1}^{N_c^{\text{eff}}} \langle T_n \rangle + \sum_{n=N_c^{\text{eff}}+1}^{N_c} \langle T_n \rangle}. \quad (71)$$

In the quasi-ballistic limit ($L \ll L_b$) the first term in the denominator of Eq. (71) is simply N_c^{eff} and the second term can be evaluated by means of Eq. (69). For $L_n = L_b$ we find

$$\langle \rho \rangle \simeq \frac{1}{N_c} + \frac{N_c - N_c^{\text{eff}}}{N_c^2 L_b} L \simeq \frac{1}{N_c} + \frac{1}{N_c L_b} L, \quad (72)$$

where the right-hand side holds for $N_c^{\text{eff}} \ll N_c$. In the diffusive regime ($l \ll L < \xi$) we evaluate the denominator of Eq. (71) by means of Eq. (69) and we neglect the second term in the denominator, assuming that $N_c^{\text{eff}} L_a \gg N_c L_b$. We get

$$\langle \rho \rangle \simeq \frac{L_a + L}{N_c^{\text{eff}} L_a} \simeq \frac{1}{N_c^{\text{eff}}} + \frac{1}{N_c^{\text{eff}} L_a} L, \quad (73)$$

where the righthand side is the limit $L \gg L_a$. This means that we assume $\langle T_n \rangle \simeq L_n/L$ for all N_c^{eff} channels, i.e., we ignore that the channel $n = 1$ is almost quasi-ballistic even at $L \simeq \xi$ (see Fig. 13). Nevertheless, we succeed in obtaining all major features of the crossover from the quasi-ballistic regime to the diffusive one (see mainly the next subsection).

If we compare the formulas (72) and (73) with the formulas $\langle \rho \rangle = \rho_c + \rho_{\text{qb}} L/W$ and $\langle \rho \rangle = \rho_c^{\text{eff}} + \rho_{\text{dif}} L/W$, we obtain

$$\rho_{\text{qb}} = \frac{W}{N_c L_b}, \quad \rho_{\text{dif}} = \frac{W}{N_c^{\text{eff}} L_a}. \quad (74)$$

We have assumed above that $N_c^{\text{eff}} L_a \gg N_c L_b$. This means that $\rho_{\text{qb}} \gg \rho_{\text{dif}}$. Indeed, we will see that $\rho_{\text{qb}}/\rho_{\text{dif}} \simeq N_c$.

Formula (73) holds only for $L \lesssim \xi$, as Eq. (70) holds for $L \lesssim \xi$. However, the formula

$$\frac{1}{\langle g \rangle} \simeq \frac{1}{N_c^{\text{eff}}} + \frac{1}{N_c^{\text{eff}} L_a} L \quad (75)$$

holds for $l \ll L \lesssim 2\xi$, as we know from our numerical data. (The fact that the conductance behaves diffusively up to $L \simeq 2\xi$ has previously been recognized from the conductance distribution.²² We do not show here the conductance distributions as they are similar to those in Refs. 22 and 24.)

Formulas (72) and (73) show that the crossover from $\langle \rho \rangle = \rho_c + \rho_{\text{qb}} L/W$ to $\langle \rho \rangle = \rho_c^{\text{eff}} + \rho_{\text{dif}} L/W$ is due to the channel nonequivalency. In what follows, formulas (72) and (73) will be derived from the first principles, without using the parameters L_a and L_b .

C. Crossover from the quasi-ballistic to diffusive transport:

Microscopic analytical derivation

We express the transmission probability $\langle T_n \rangle$ as

$$\langle T_n \rangle = 1 - \sum_{m=1}^{N_c} \langle R_{mn} \rangle. \quad (76)$$

where R_{mn} is the probability that an electron impinging on the disordered region in the m th channel is reflected back into the n th channel. In Ref. 20 the wire with rough edges was analyzed in the quasi-ballistic limit and the reflection probability $\langle R_{mn} \rangle$

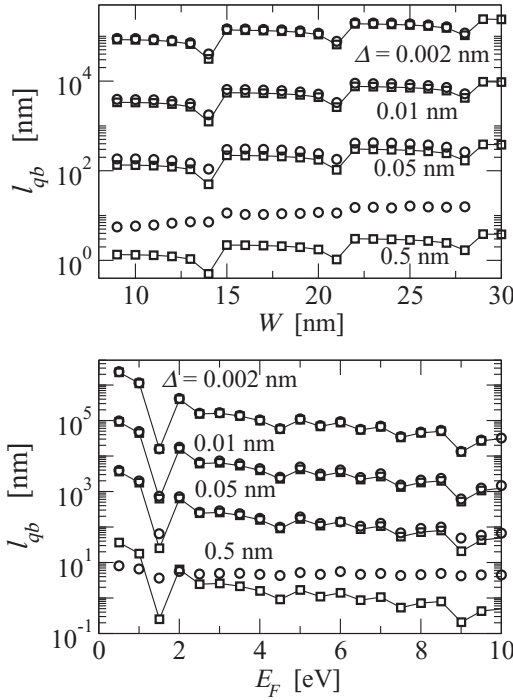


FIG. 14. Top panel: Quasi-ballistic mean free path l_{qb} in the Au wire as a function of the wire width W for various roughness amplitudes Δ . The roughness correlation length is fixed at $\Delta x = 0.125$ nm, the Au material parameters are $m = 9.109 \times 10^{-31}$ kg and $E_F = 5.6$ eV. The circles show our numerical data and the squares (connected by a solid line) are the data points obtained from expression (79). Bottom panel: The same calculations as in the top panel, but W is fixed at 9 nm and the Fermi energy is varied. To explore the small Δ limit reliably, we have to use the values of Δ , which are too small to be realistic.

was derived by means of first-order perturbation theory. The result is

$$\langle R_{mn} \rangle = 2 \times \frac{\delta^2 \kappa_m^2 \kappa_n^2}{W^2 k_m k_n} \mathcal{F}(|k_n + k_m|) L, \quad (77)$$

where $\kappa_n = (\pi/W)n$ and the factor of 2 accounts for two edges. [In fact, the result given in Ref. 20 involves a missprint. The result in Eq. (77) can also be extracted from the backscattering length reported in Refs. 40 and 41.]

The mean conductance in the quasi-ballistic limit reads

$$\langle g \rangle = \sum_{n=1}^{N_c} \left[1 - \sum_{m=1}^{N_c} \langle R_{mn} \rangle \right] = N_c \left[1 - \frac{L}{\frac{\pi}{2} l_{qb}} \right], \quad (78)$$

where l_{qb} is the quasi-ballistic mean free path:

$$l_{qb} = \frac{2}{\pi} N_c \left[\sum_{m=1}^{N_c} \sum_{n=1}^{N_c} \frac{2\Delta^2 \kappa_m^2 \kappa_n^2}{3W^2 k_m k_n} \mathcal{F}(|k_n + k_m|) \right]^{-1}, \quad (79)$$

where $\delta^2 = \Delta^2/3$. Note that the quasi-ballistic limit of Eq. (79) contains only the backscattering contribution $\propto \mathcal{F}(|k_n + k_m|)$, while in the diffusive regime [Eq. (64)] also

the forward-scattering contribution $\propto \mathcal{F}(|k_n - k_m|)$ is also present. The mean resistance in the quasi-ballistic limit is

$$\langle \rho \rangle = \frac{1}{\langle g \rangle} = \frac{1}{N_c} + \frac{1}{N_c \frac{\pi}{2} l_{qb}} L. \quad (80)$$

In Fig. 14 expression (79) is compared with l_{qb} determined numerically by means of the approach discussed in Fig. 7 (the right panel and inset to the right panel). Formula (79) agrees with our numerical data if the roughness amplitude Δ is small. This is what one expects, because perturbation expression (79) is exact in the limit $\Delta \rightarrow 0$ and our scattering-matrix calculation is (in principle) exact for any Δ . As Δ increases, the result of Eq. (79) fails to agree with our numerical data because the scattering is not weak.⁴²

Simple formulas can be derived for l_{qb} and l if the roughness is uncorrelated ($\Delta x/\lambda_F \ll 1$). We start with l . If $\Delta x/\lambda_F \ll 1$, correlation function (68) is simply $\mathcal{F}(q) = \Delta x$. Consequently, the backscattering and forward-scattering terms in Eq. (64) become the same and matrix (64) reduces to the diagonal form

$$K_{nn'} = \delta_{nn'} \frac{2\pi^2 \Delta^2 \Delta x}{3W^6} \sum_{\mu=1}^{N_c} n^2 \mu^2 \frac{k_n}{k_\mu}, \quad (81)$$

where the factor of 2 is just due to the equal contribution of the backward and forward scattering. We set Eq. (81) into the Boltzmann conductivity of Eq. (59) and we extract from Eq. (59) the diffusive mean free path. It reads

$$l = \frac{3W^5}{\pi^4 \Delta^2 k_F \Delta x} \sum_{n=1}^{N_c} \frac{k_n}{n^2} \left[\sum_{\mu=1}^{N_c} \frac{\mu^2}{k_\mu} \right]^{-1}. \quad (82)$$

For $N_c \gg 1$ the summations in Eq. (82) can be approximated as

$$\sum_{n=1}^{N_c} \frac{k_n}{n^2} \simeq \frac{\pi^2}{6} k_F, \quad \sum_{\mu=1}^{N_c} \frac{\mu^2}{k_\mu} \simeq \frac{W^3}{4\pi^2} k_F^2, \quad (83)$$

and the semiclassical diffusive mean free path becomes

$$l = \frac{2W^2}{\Delta^2 k_F^2 \Delta x}. \quad (84)$$

Now we evaluate for $\Delta x/\lambda_F \ll 1$ the quasi-ballistic mean free path. We rewrite Eq. (79) in the form

$$l_{qb} = \frac{2}{\pi} N_c \left[\sum_{m=1}^{N_c} \sum_{n=1}^{N_c} \frac{1}{l_{mn}^R} \right]^{-1}, \quad (85)$$

where

$$\frac{1}{l_{mn}^R} = \frac{2\Delta^2 \kappa_m^2 \kappa_n^2}{3W^2 k_m k_n} \mathcal{F}(|k_n + k_m|). \quad (86)$$

Setting into Eq. (86) the formula $\mathcal{F}(q) = \Delta x$, we obtain

$$l_{mn}^R = \frac{3W^2 k_m k_n}{2\Delta^2 \kappa_m^2 \kappa_n^2 \Delta x} = \frac{3W^6 k_m k_n}{2\pi^4 \Delta^2 m^2 n^2 \Delta x}. \quad (87)$$

Combining Eq. (85) with Eq. (87) and using Eq. (83) we obtain

$$l_{qb} = \frac{2}{\pi} \frac{24W}{\pi \Delta^2 k_F^3 \Delta x}. \quad (88)$$

We recall that l_{qb} is limited exclusively by backscattering.

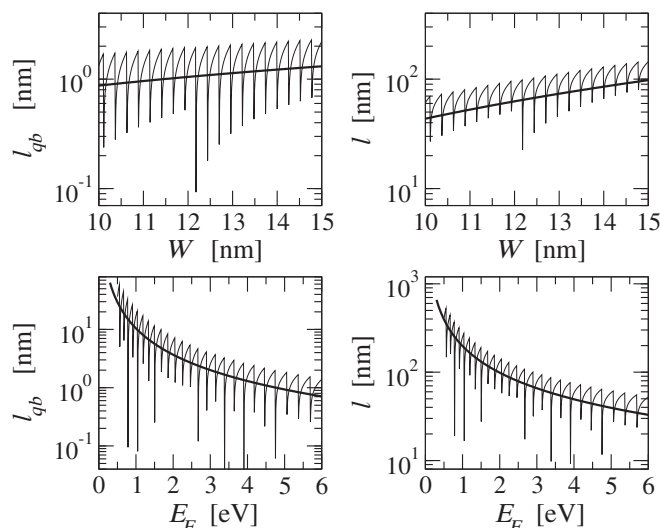


FIG. 15. Quasi-ballistic mean free path l_{qb} and diffusive mean free path l in the Au wire with rough edges, calculated as a function of the wire width W and Fermi energy E_F . The thick lines show formulas (88) and (84), derived for the uncorrelated roughness. The thin lines show the formulas valid for an arbitrary correlation length Δx , namely the quasi-ballistic result of Eq. (79) and the semiclassical l extracted from the Boltzmann conductivity of Eq. (59). The roughness amplitude Δ and roughness-correlation length Δx are fixed as $\Delta = 0.5$ nm and $\Delta x = 0.125$ nm (the limit $\Delta x/\lambda_F \ll 1$ is fulfilled for all considered data). The Fermi energy used in the top panels is $E_F = 5.6$ eV, the wire width in the bottom panels is $W = 9$ nm. The oscillations with sharp minima appear whenever the Fermi energy approaches the bottom of the energy subband $n = N_c$.

Formulas (84) and (88) hold for $\Delta x/\lambda_F \ll 1$. In Fig. 15 we compare them with the original formulas valid for any Δx . We can see that the major difference is the absence of the oscillating behavior in formulas (84) and (88).

Finally, the ratio l/l_{qb} can be expressed as

$$\frac{l}{l_{qb}} = \frac{\pi^3}{24} N_c \sim N_c. \quad (89)$$

The result of Eq. (89) is universal—independent of the wire parameters and parameters of disorder. Figure 16 shows that the universal relation $l/l_{qb} \propto N_c$ is confirmed by our exact quantum-transport calculation. Obviously, since formula (84) is the semiclassical Boltzmann equation result and formula (88) is the weak-scattering limit, formula (89) cannot reproduce the exact quantum results quantitatively.

The diffusive mean free path of Eq. (84) contains both the backward and forward scattering. It is therefore interesting that the same result can be obtained when the quasi-ballistic (backward-scattering-limited) resistance of Eq. (80) is extrapolated into the diffusive regime by means of ansatz (69). We start from

$$\langle \rho \rangle \simeq 1/\langle g \rangle = \left[\sum_{n=1}^{N_c} \langle T_n \rangle \right]^{-1} \quad (90)$$

and we use ansatz (69). In the quasi-ballistic limit ($L \ll L_n$) we obtain from Eq. (69) the formula $\langle T_n \rangle = 1 - L/L_n$. We

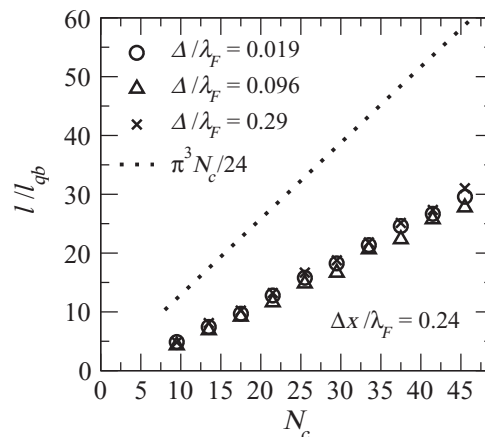


FIG. 16. Ratio l/l_{qb} , where l is the diffusive mean free path and l_{qb} is the quasi-ballistic mean free path, evaluated as a function of N_c for various roughness amplitudes Δ . The roughness-correlation length Δx is fixed to the value $\Delta x/\lambda_F = 0.24$, which reasonably emulates the uncorrelated roughness. The open symbols show the results of our quantum transport simulation, where l and l_{qb} are calculated as in Fig. 7.

set this formula into Eq. (90) and we compare Eq. (90) with quasi-ballistic expressions (80) and (85). We find that

$$L_n = \left[\sum_{m=1}^{N_c} \frac{1}{l_{mn}^R} \right]^{-1}. \quad (91)$$

In the diffusive limit ($L_n \ll L$) we obtain from Eq. (69) the formula $\langle T_n \rangle = L_n/L$ and from Eq. (90) the diffusive expression

$$\langle \rho \rangle = \left[\sum_{n=1}^{N_c} L_n \right]^{-1} L. \quad (92)$$

We compare this expression with $\rho = \rho_{\text{dif}} \frac{L}{W}$, where $\rho_{\text{dif}} = 2/(k_F l)$. We find the mean free path

$$l = \frac{2}{\pi N_c} \sum_{n=1}^{N_c} L_n = \frac{2}{\pi N_c} \sum_{n=1}^{N_c} \left[\sum_{m=1}^{N_c} \frac{1}{l_{mn}^R} \right]^{-1}. \quad (93)$$

If we set into Eq. (93) the uncorrelated limit of Eq. (87), we obtain again the Boltzmann mean free path (84). This is the proof that ansatz (69) works correctly for the uncorrelated roughness. Now it is useful to make two remarks.

First, our characteristic length L_n should not be confused with the often-used^{41,43} attenuation length L_n . Our L_n is defined by ansatz (69) and we have just seen that expression (93) gives for such L_n the mean free path coinciding with the mean free path obtained from the Boltzmann equation. This is the momentum relaxation-time-limited mean free path. However, if one sets into Eq. (93) the attenuation length [Eq. (5.2) in Ref. 43], one obtains from Eq. (93) the scattering-time-limited mean free path, i.e., the mean distance between two subsequent collisions. For the uncorrelated roughness the latter is exactly twice as shorter as the former one.

Second, we note that ansatz (69) does not work for arbitrary roughness. Indeed, we can set into formula (93) the more general expression (86) and we can compare Eq. (93) with the

Boltzmann mean free path valid for an arbitrary correlation length Δx . In such a case formula (93) fails to reproduce the Boltzmann equation result.

Assuming the uncorrelated roughness, we are ready to derive analytically the effective number of the open channels, N_c^{eff} . Expression (90) can be formally written as

$$\langle \rho \rangle = \frac{1}{N_c^{\text{eff}}} + \frac{2}{k_F l} \frac{L}{W}, \quad (94)$$

where the symbol N_c^{eff} is defined as

$$N_c^{\text{eff}} = \left[\left(\sum_{n=1}^{N_c} \langle T_n \rangle \right)^{-1} - \frac{2}{\pi N_c l} L \right]^{-1} \quad (95)$$

in order to obtain Eq. (90) again. We now express the transmission $\langle T_n \rangle$ by means of formula (69) and the mean free path l by means of formula (93). We obtain

$$N_c^{\text{eff}} = \left[\left(\sum_{n=1}^{N_c} \frac{L_n}{L_n + L} \right)^{-1} - \left(\sum_{n=1}^{N_c} L_n \right)^{-1} L \right]^{-1}. \quad (96)$$

In the diffusive limit ($L \gg L_n$) we obtain after some algebraic manipulations the equation

$$N_c^{\text{eff}} = \frac{\left(\sum_{n=1}^{N_c} L_n \right)^2}{\sum_{n=1}^{N_c} L_n^2}. \quad (97)$$

Expression (97) no longer depends on L and evidently represents the effective number of the open channels, if the resistance of Eq. (94) is considered in the diffusive limit. We set into Eq. (97) formulas (91) and (87). We obtain

$$N_c^{\text{eff}} = \frac{\left[\sum_{n=1}^{N_c} \frac{k_n}{n^2} \right]^2 \left[\sum_{m=1}^{N_c} \frac{m^2}{k_m} \right]^{-2}}{\left[\sum_{n=1}^{N_c} \frac{k_n^2}{n^4} \right] \left[\sum_{m=1}^{N_c} \frac{m^2}{k_m} \right]^{-2}}. \quad (98)$$

For $N_c \gg 1$ the first sum in the denominator of Eq. (98) becomes

$$\sum_{n=1}^{N_c} \frac{k_n^2}{n^4} \simeq \frac{\pi^4}{90} k_F^2, \quad (99)$$

and other sums in Eq. (98) are already known [see Eqs. (83)]. We arrive at the result

$$N_c^{\text{eff}} \simeq \frac{5}{2}, \quad (100)$$

which implies that N_c^{eff} is a universal number depending on neither the roughness amplitude Δ nor on the number of the conducting channels, N_c . All this agrees with our quantum-transport calculation in Fig. 12, except that the result of Eq. (100) underestimates the numerical value $N_c^{\text{eff}} \simeq 6$ about twice. However, we recall that the result of Eq. (100) relies on formulas (91) and (87), which are not exact.

D. Diffusive mean free path: Quantum-transport results versus the semiclassical Boltzmann results

In this subsection, the mean free path obtained from the semiclassical Boltzmann equation is compared with the mean free path obtained from the quantum resistivity ρ_{dir} . For the impurity disorder we see a standard result:^{6,7} The semiclassical

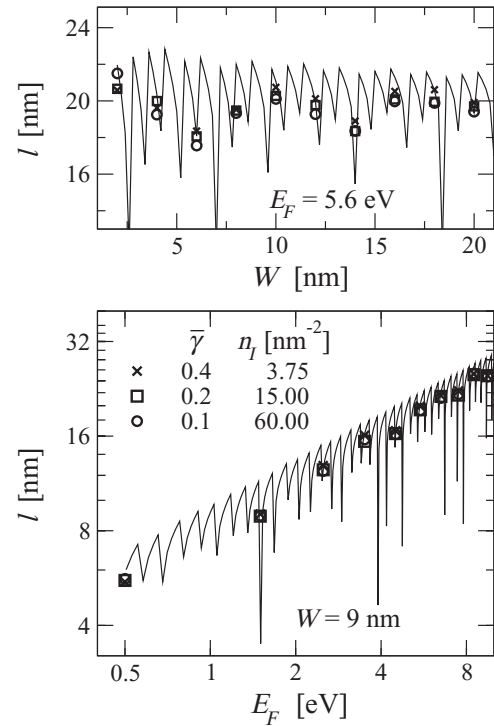


FIG. 17. Top panel: Diffusive mean free path l in the Au wire with impurity disorder as a function of the wire width W , calculated for three different sets of impurity parameters (listed in the bottom panel). The semiclassical mean free path obtained from the Boltzmann Q1D conductivity Eq. (62) is shown as a solid line: All three sets of parameters are intentionally chosen to give the same semiclassical result. The data shown by symbols are the quantum-transport results obtained from the quantum resistivity ρ_{dir} (by using the procedure described in Fig. 7). Bottom panel: The same calculations as in the top panel, but W is fixed at 9 nm and the Fermi energy is varied.

and quantum mean free paths coincide for weak impurities. On the contrary, for the edge roughness we find that the quantum mean free path differs from the semiclassical one even if the roughness amplitude Δ is vanishingly small.

In Fig. 17 the quantum and semiclassical mean free paths are compared for the impurity disorder. The semiclassical data are shown in a solid line: Three different sets of parameters are intentionally chosen to provide the same semiclassical result. The full lines exhibit oscillations with sharp minima, appearing whenever the Fermi energy approaches the bottom of the energy subband $n = N_c$. Evidently, the oscillating curve intersects the quantum results (the data shown by symbols), albeit they are slightly affected by statistical noise. Both the semiclassical and quantum results follow the trend predicted by the semiclassical 2D limit [Eq. (63)], namely that l is proportional to $E_F^{1/2}$ and independent of W . In summary, in the Q1D wire with impurity disorder the semiclassical and quantum mean free paths coincide. This is a standard result,^{6,7} known from the theory based on the white-noise disorder³ (see, however, Ref. 44).

As shown in Fig. 18, in the wire with rough edges the situation is different. We again compare the semiclassical mean free path (solid lines) with the quantum mean free path (open circles). As before, the solid lines exhibit oscillations

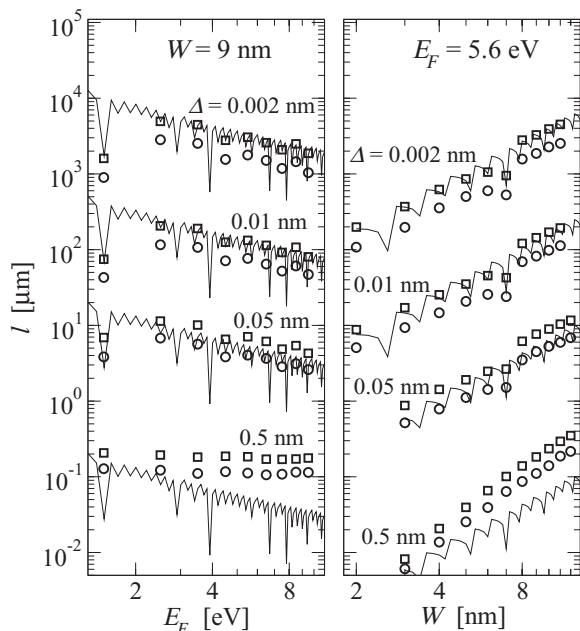


FIG. 18. The right panel shows the diffusive mean free path l in the Au wire with rough edges as a function of the wire width W , calculated for various roughness amplitudes Δ . The left panel shows the same calculation, but W is fixed at 9 nm and the Fermi energy is varied. The roughness-correlation length is kept at the value $\Delta x = 0.125$ nm, which means that $\Delta x/\lambda_F \lesssim 1$ for most of the presented data. The solid lines show the semiclassical mean free path obtained from the Boltzmann Q1D conductivity [Eqs. (59) and (64)]. The open circles show the quantum mean free path extracted from the quantum resistivity ρ_{dif} (by using the procedure described in Fig. 7). The open squares show the mean free path obtained by means of the classical scattering-matrix calculation (see the text), in which the localization is absent. To explore the small Δ limit reliably, we have to use values of Δ which are too small to be realistic.

with sharp minima, appearing whenever the Fermi energy approaches the bottom of the energy subband $n = N_c$. Evidently, the solid line and open circles show a quite different behavior if the roughness amplitude Δ is large (notice the results for $\Delta = 0.5$ nm). It is tempting to ascribe this difference to the weak-perturbation approximation involved in the Boltzmann equation, and, similarly, it is tempting to expect that the full line will intersect the open circles for sufficiently small Δ . However, this is not the case: Even for the smallest considered Δ the open circles are systematically a factor of ~ 2 below the solid line. In summary, in the wire with rough edges the quantum mean-free path differs from the semiclassical one (by the factor of ~ 2) even if Δ is vanishingly small.

To understand the origin of this difference, we now exclude from our quantum-transport calculation the wave interference. We recall (see Sec. II C) that in the quantum-transport calculation the total S matrix of the disordered wire is obtained by combining at random the scattering matrices (b_i) of the building blocks, where the $2N \times 2N$ matrix b_i is composed of the complex amplitudes t_{mn}, t'_{mn}, r_{mn} , and r'_{mn} . To exclude the wave interference, we proceed as follows.⁷ First, we consider only the conducting channels and we completely neglect the evanescent ones: This reduces the size of the

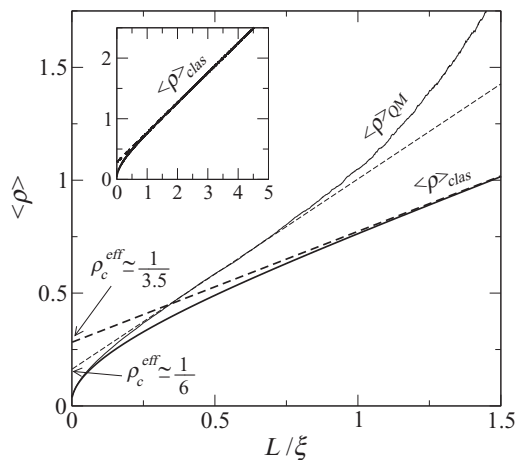


FIG. 19. Mean resistance $\langle \rho \rangle$ of the wire with rough edges in dependence on the ratio L/ξ . The thin solid line is the result of the quantum scattering-matrix calculation (the same data as in the top right panel of Fig. 9), now labeled as $\langle \rho \rangle_{QM}$. The thick solid line is the result of the classical scattering-matrix calculation, labeled as $\langle \rho \rangle_{\text{clas}}$. The dashed lines show the linear fits $\langle \rho \rangle = \rho_c^{\text{eff}} + \rho_{\text{dif}} L/W$, from which we determine the effective contact resistance ρ_c^{eff} and the diffusive mean free path $l = 2/(k_F \rho_{\text{dif}})$. The resulting ρ_c^{eff} are shown in the figure. The inset shows the classical result again, but for larger L/ξ in order to stress the linear raise and absence of the localization.

matrix b_i to $2N_c \times 2N_c$. Second, instead of the complex matrix b_i we use the real one, in which the complex amplitudes t_{mn}, t'_{mn}, r_{mn} , and r'_{mn} are replaced by the real probabilities $T_{mn} = |t_{mn}|^2, T'_{mn} = |t'_{mn}|^2, R_{mn} = |r_{mn}|^2$, and $R'_{mn} = |r'_{mn}|^2$, respectively. Of course, the wave interference is excluded completely if the length of the building block, L_b , coincides with the length of the edge step, Δx . Fortunately, in practical calculations the wave interference is negligible already for $L_b \sim l$. If we combine the resulting real matrices b_i by means of the same combination law as before [Eq. (24)], we obtain the classical transmission probability \mathcal{T}_{mn} and eventually the classical Landauer conductance

$$g_{\text{clas}} = \sum_{m=1}^{N_c} \sum_{n=1}^{N_c} \mathcal{T}_{mn} \frac{k_m}{k_n}. \quad (101)$$

Finally, we perform ensemble averaging over many samples.

In Fig. 19 the classical scattering-matrix calculation is compared with the quantum one. The mean resistance due to the quantum calculation is labeled as $\langle \rho \rangle_{QM}$ to distinguish it from the classical $\langle \rho \rangle_{\text{clas}}$. It can be seen that both $\langle \rho \rangle_{QM}$ and $\langle \rho \rangle_{\text{clas}}$ exhibit the crossover to the linear diffusive dependence $\langle \rho \rangle = \rho_c^{\text{eff}} + \rho_{\text{dif}} L/W$, but the classical result shows a smaller value of ρ_{dif} and a larger value of ρ_c^{eff} . The value $\rho_c^{\text{eff}} = 1/N_c^{\text{eff}} \simeq 1/3.5$ is already close to our theoretical result $N_c^{\text{eff}} \simeq 2.5$ [Eq. (100)], where the wave interference is excluded as well. The smaller value of ρ_{dif} is due to the absence of the localization.

Let us return to Fig. 18. The squares show the mean free path extracted from $\langle \rho \rangle_{\text{clas}}$. These data overestimate the quantum results (circles) systematically by a factor of ~ 2 . Compare now the classical scattering-matrix results (squares) with the semiclassical Boltzmann results (solid lines). The solid lines intersect the squares only if Δ is vanishingly small.

TABLE I. The mean-free path l in the Au wire obtained from the quantum-transport simulation is compared with the semiclassical Boltzmann mean-free path l_{Boltz} [Eqs. (59) and (64)] for various values of the wire width W , roughness amplitude Δ , and roughness-correlation length Δx . Each set of the parameters considered in the table represents strong disorder, for which l_{Boltz} strongly differs from l .

W (nm)	Δx (nm)	Δ (nm)	l (nm)	l_{Boltz} (nm)
9	0.5	1.5	21.4	5.17
20	10	3.33	70.7	21.3
20	5	3	65.6	17.2
30	2.5	4	124	14.8
30	5	4.5	105	16.6
70	5	10.5	315	20.5
90	5	13.5	409	30.0
90	40	13.5	411	115

This is due to the fact that the Boltzmann results rely on the weak perturbation theory while the classical scattering-matrix calculation still involves the exact quantum scattering by a single edge step.

The roughness-limited conductivity derived from the Boltzmann equation (usually further simplified by using the Fuchs–Sondheimer model^{45,46}) is often compared with the transport measurements of the metallic nanowires.^{47–49} However, such comparison cannot verify the Boltzmann result unambiguously due to the presence of other processes (like the scattering by impurities and grain boundaries) and also due to the fact that the roughness parameters Δ and Δx are not known *a priori*. Our quantum calculation shows unambiguously that the semiclassical Boltzmann approach describes the wires with rough edges reasonably, only if Δ is too small to be realistic (in the Au nanowires). In practice, the metallic nanowires are usually fabricated by advanced lift-off techniques,^{50–52} which hardly allow suppressing the edge roughness to the value $\Delta \sim 1$ nm.

In Table I, the quantum and semiclassical mean free paths are compared for a more realistic Δ and W as in Fig. 18. We see that the quantum result exceed the semiclassical Boltzmann result by one order of magnitude. One might argue that the quantum result holds only in the coherent regime while decoherence is present at any nonzero temperature. We expect that decoherence will tend to destroy the wave interference and to restore the resistance $\langle \rho \rangle_{\text{clas}}$ resulting from the classical scattering-matrix approach. The resulting classical mean free path would be twice as large as the quantum one [see Fig. 18], i.e., it would exceed the Boltzmann mean free path in Table I by another factor of 2.

E. Wires with strongly correlated edge roughness: $\Delta x/\lambda_F \gg 1$

The wires with rough edges have so far been discussed for the roughness-correlation lengths $\Delta x \lesssim \lambda_F$. The only exception was the Fig. 12, where the effective number of the open channels, N_c^{eff} , was calculated from $\Delta x \ll \lambda_F$ up to $\Delta x \gg \lambda_F$. We have seen, that the value of N_c^{eff} approaches for $\Delta x \gg \lambda_F$ the value of N_c , which suggests that the

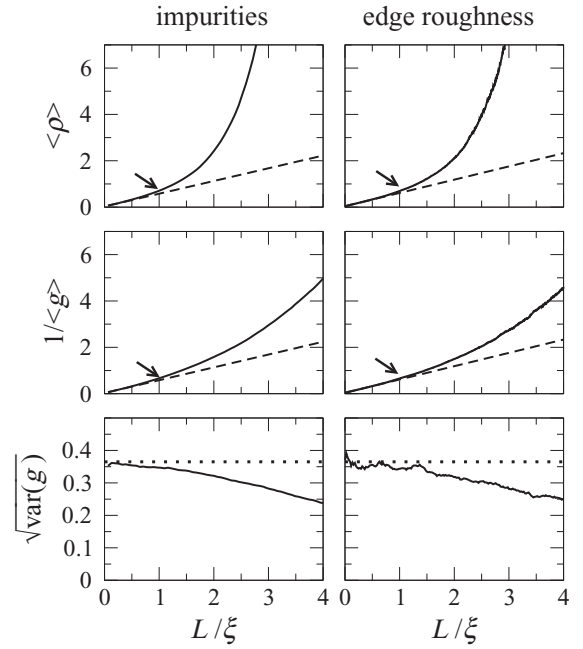


FIG. 20. The same calculation and the same symbols as in Fig. 9, except that the edge roughness is considered in the limit $\Delta x/\lambda_F \gg 1$. Specifically, the data obtained for the wire with impurities (left column) are the same as those in the left column of Fig. 9, while for the edge roughness (right column) we show the data obtained for $\Delta x/\lambda_F = 19\,300$ and $\Delta/\lambda_F = 0.096$ (the data for $\Delta/\lambda_F = 0.019$ and $\Delta/\lambda_F = 0.96$, not shown, look similar except for statistical noise). We recall that the localization length ξ is determined from the dependence $\langle \ln g \rangle = -L/\xi$. For the edge roughness we now obtain $\xi/l \simeq 0.92N_c$, which is close to the impurity case: $\xi/l \simeq 0.88N_c$.

diffusive dependence $\langle \rho \rangle = 1/N_c^{\text{eff}} + \rho_{\text{dif}}L/W$ approaches the standard form $\langle \rho \rangle = 1/N_c + \rho_{\text{dif}}L/W$, seen in the wire with impurities. In this subsection we focus on the limit $\Delta x \gg \lambda_F$.

Figure 20 shows the same calculations as Fig. 9, except that the wire with rough edges is now simulated in the limit $\Delta x \gg \lambda_F$. Unlike Fig. 9, the results for the wire with rough edges are now close to the results for the wire with impurity disorder.

First, the localization length in the wire with rough edges fulfills the relation $\xi/l \simeq 0.92N_c$, which is close to the relation $\xi/l \simeq 0.88N_c$ found for the impurity disorder. This is why the resistance $\langle \rho \rangle$ and inverse conductance $1/\langle g \rangle$ in Fig. 20 show for both types of disorder the same linear slope with L/ξ . Moreover, the same linear slope means a single linear regime for the quasi-ballistic as well as diffusive transport, i.e., the crossover between the quasi-ballistic and diffusive regimes, observed for $\Delta x \lesssim \lambda_F$, tends to disappear. (In Fig. 9 a remarkably larger slope is seen for the edge roughness because $\xi/l \simeq 1.4N_c$.)

Second, the inverse conductance in Fig. 20 shows for both types of disorder the linear diffusive regime for $L/\xi < 1$ and onset of localization for $L/\xi \simeq 1$. (In Fig. 9 the inverse conductance of the wire with rough edges shows the onset of localization for $L/\xi \simeq 2$.)

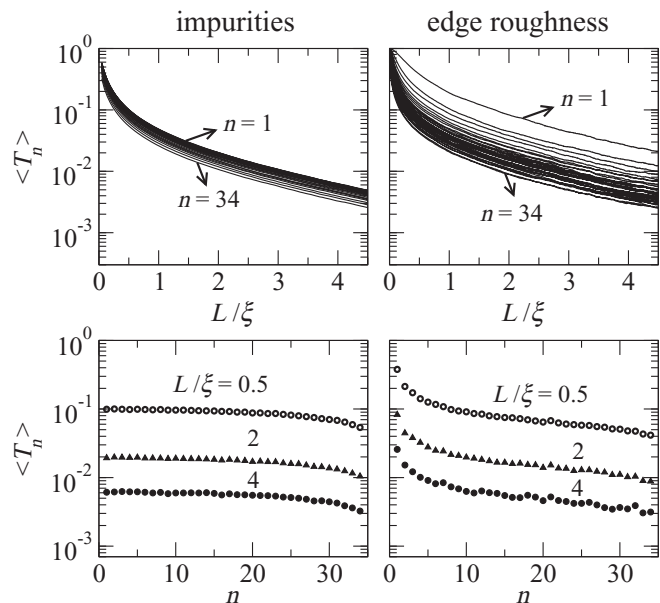


FIG. 21. The same calculation and the same symbols as in Fig. 13, except that the edge roughness is considered in the limit $\Delta x/\lambda_F \gg 1$ (we show the data for $\Delta x/\lambda_F = 19\,300$).

Third, the wire with rough edges now exhibits essentially the same universal conductance fluctuations as the wire with impurities. The size of these fluctuations is in accord with the value $\sqrt{\text{var}(g)} = 0.365$, predicted for the white-noise-like disorder. To see such conductance fluctuations for the edge roughness is surprising: So far only the value $\sqrt{\text{var}(g)} \simeq 0.3$ has been reported.^{9,25,27,28}

To provide insight, it is useful to look at the transmission probabilities $\langle T_n \rangle$. Figure 21 shows the same calculation as Fig. 13, but with the edge roughness considered in the limit $\Delta x/\lambda_F \gg 1$. It can be seen that Fig. 21 differs from Fig. 13 in the following respect: Except for a few channels with the lowest values of n , the wire with rough edges and the wire with impurities show for the rest of the channels a very similar $\langle T_n \rangle$, which is clearly not the case in Fig. 13. This similarity is responsible for the similarity of the transport results in Fig. 20. The observed similarity could be further improved by simulating the wires with N_c larger than 34, but this is beyond the scope of this work.

Finally, Fig. 22 shows for $\Delta x \gg \lambda_F$ what happens in the wire with rough edges with the diffusive mean free path. Specifically, the semiclassical Boltzmann result (solid lines) is compared with the quantum (open circles) and classical (open squares) scattering-matrix calculations. In the limit $\Delta x \gg \lambda_F$ all three calculations tend to give the same mean free path. This means that the interference effects observed for $\Delta x \lesssim \lambda_F$ are no longer important, or, in other words, the diffusive transport in the wire with rough edges is semiclassical. This is again similar to the wire with impurities.

For $\Delta x \gg \lambda_F$ it is easy to show analytically that the semiclassical Boltzmann mean free path rises with Δx linearly. The correlation function $\mathcal{F}(q)$ contains the function $\cos(\Delta x q)$. This function oscillates with q at random and the oscillations become very fast for $\Delta x \gg \lambda_F$. Consequently, the correlation

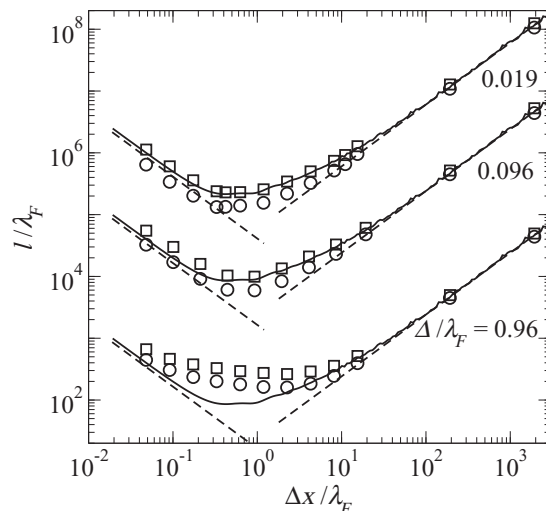


FIG. 22. Diffusive mean free path l in the wire with rough edges as a function of the roughness-correlation length Δx for various roughness amplitudes Δ , with l , Δx , and Δ scaled by λ_F . The wire width W is fixed to the value $W/\lambda_F = 17.4$, which means that $N_c = 34$. The solid lines show the semiclassical mean free path obtained from the Boltzmann conductivity [Eqs. (59) and (64)]. The dashed lines for $\Delta x/\lambda_F \lesssim 1$ show the uncorrelated limit of Eq. (84), the dashed lines for $\Delta x/\lambda_F \gtrsim 1$ show the correlated limit of Eqs. (102). The circles show the quantum mean free path extracted from the quantum resistivity ρ_{dif} (by using the procedure described in Fig. 7). The squares show the mean free path obtained by means of the classical scattering-matrix calculation in which the localization effect is absent (see Sec. IV D). Note that for the Au wire ($E_F = 5.6$ eV and $m = 9.109 \times 10^{-31}$ kg) we have $\lambda_F = 0.52$ nm, i.e., the wire width is $W = 17.4\lambda_F = 9$ nm and the smallest Δ is only 0.01 nm. Such small Δ is obviously not realistic, which demonstrates an important finding: The semiclassical Boltzmann result (solid line) reproduces the classical scattering-matrix calculation (squares) for any Δx only if Δ is too small to be realistic.

function $\mathcal{F}(q)$ oscillates fast around the value $\mathcal{F}(q) = \frac{2}{q^2 \Delta x}$. If we ignore these fast oscillations, the diffusive mean free path can be written as

$$l = \frac{3\Delta x W^5}{k_F \pi^4 \Delta^2} \sum_n \sum_{n'}^{N_c} k_n k_{n'} (\mathcal{K}^{-1})_{nn'} \quad (102)$$

where

$$\mathcal{K}_{nn'} = \delta_{nn'} \left[\sum_{\mu \neq n}^{N_c} n^2 \mu^2 \frac{k_n}{k_\mu} \left[\frac{1}{(k_\mu - k_n)^2} + \frac{1}{(k_\mu + k_n)^2} \right] + \frac{n^4}{2k_n^2} \right] - (1 - \delta_{nn'}) n^2 n'^2 \left[\frac{1}{(k_{n'} - k_n)^2} - \frac{1}{(k_{n'} + k_n)^2} \right]. \quad (103)$$

It can be seen that $l \propto \Delta x$. The $l \propto \Delta x$ dependence resembles the wire with impurities, where l rises linearly with the average distance between the impurities. Formula (102) is plotted in Fig. 22 as a dashed line. It indeed agrees with the numerical data for $\Delta x \gg \lambda_F$. On the other hand, the formula (84), derived in the opposite limit, reasonably agrees with the

numerical data for $\Delta x \ll \lambda_F$, but the dependence $l \propto 1/\Delta x$ has no similarity with the impurity case.

Finally, as also pointed out in the figure caption, Fig. 22 shows that the semiclassical Boltzmann result (solid line) reproduces the classical scattering-matrix calculation (squares) for any Δx only if Δ is too small to be realistic. This is another indication that the Boltzmann equation theory of the edge-roughness-limited transport should be used with caution, at least in the Au nanowires.

V. SUMMARY AND CONCLUDING REMARKS

We have studied quantum transport in Q1D wires made of a conductor of width W and length $L \gg W$. The main purpose of our paper was to compare an impurity-free wire with rough edges with a smooth wire with impurity disorder. We have calculated the electron transmission through the wires by the scattering-matrix method, and we have obtained the Landauer conductance and resistance for a large ensemble of macroscopically identical disordered wires.

We first studied the impurity-free wire whose edges have a roughness correlation length comparable with the Fermi wavelength. The mean resistance $\langle \rho \rangle$ and inverse mean conductance $1/\langle g \rangle$ have been evaluated as depending on L . For $L \rightarrow 0$ we have found the quasi-ballistic dependence $1/\langle g \rangle = \langle \rho \rangle = 1/N_c + \rho_{\text{qb}}L/W$, where $1/N_c$ is the fundamental contact resistance and ρ_{qb} is the quasi-ballistic resistivity. For larger L we have found the crossover to the diffusive dependence $1/\langle g \rangle \simeq \langle \rho \rangle = 1/N_c^{\text{eff}} + \rho_{\text{dif}}L/W$, where ρ_{dif} is the resistivity and $1/N_c^{\text{eff}}$ is the effective contact resistance corresponding to the N_c^{eff} open channels. We have found the universal results $\rho_{\text{qb}}/\rho_{\text{dif}} \simeq 0.6N_c$ and $N_c^{\text{eff}} \simeq 6$ for $N_c \gg 1$.

Approaching the localization regime, we have demonstrated the following numerical finding: As L exceeds the localization length ξ , the resistance shows onset of localization while the conductance shows the diffusive dependence $1/\langle g \rangle \simeq 1/N_c^{\text{eff}} + \rho_{\text{dif}}L/W$ up to $L \simeq 2\xi$ and the localization for $L > 2\xi$ only. On the other hand, for the impurity disorder we have found a standard diffusive behavior, namely $1/\langle g \rangle \simeq \langle \rho \rangle \simeq 1/N_c + \rho_{\text{dif}}L/W$ for $L < \xi$. We have also seen that the impurity disorder and edge roughness show the universal conductance fluctuations of different sizes, as already reported in previous works.^{9,25,27,28}

We have then attempted to interpret our quantum-transport results in terms of an approximate but microscopic analytical theory. In particular, the crossover from $1/\langle g \rangle = \langle \rho \rangle = 1/N_c + \rho_{\text{qb}}L/W$ to $1/\langle g \rangle \simeq \langle \rho \rangle = 1/N_c^{\text{eff}} + \rho_{\text{dif}}L/W$ in the wire with rough edges has been derived analytically assuming the uncorrelated edge roughness and neglecting the localization effects. In spite of this approximation, our analytical results capture the main features of our numerical results. Specifically, we have derived the universal results $\rho_{\text{qb}}/\rho_{\text{dif}} = \frac{\pi^3}{24}N_c$ and $N_c^{\text{eff}} \simeq 2.5$.

We have also derived the wire conductivity from the semiclassical Boltzmann equation, and we have compared the semiclassical mean free path with the mean free path obtained from the quantum resistivity ρ_{dif} . For the impurity disorder we have found that the semiclassical and quantum mean free paths coincide, which is a standard result. However, for the edge roughness the semiclassical mean free path strongly differs

from the quantum one, showing that the diffusive transport in the wire with rough edges is not semiclassical. We have found that it becomes semiclassical only if the roughness-correlation length is much larger than the Fermi wavelength. In such a case the resistance and conductance tend to scale with L/ξ as in the wire with impurity disorder, also showing the universal conductance fluctuations of similar size.

We end with a remark about our edge roughness model. It is the same model as in previous simulations.^{8–10,21–23} We believe that most of the results obtained within the model are model independent. For example, we have tested the correlation function $\mathcal{F}(q)$ of Gaussian shape, and we have seen that the resulting transmissions remain quite similar to those in Figure (13). The only exception is the correlated limit of Eq. (102), which predicts the dependence $l \propto \Delta x$. This dependence is the artifact of our $\mathcal{F}(q)$ choice. For example, for the Gaussian correlation function, the dependence $l \propto \Delta x$ is replaced by a much faster increase with Δx . On the other hand, the uncorrelated limit of Eq. (84) can be equally well derived for the Gaussian correlation function or for the exponential one, i.e., the result of Eq. (84) is very general.

ACKNOWLEDGMENT

We are thankful for grant No. VVCE-0058-07, VEGA Grant No. 2/0633/09, and Grant No. APVV-51-003505. We thank Peter Markoš for useful discussions in the initial stage of this work and for helpful comments to the manuscript.

APPENDIX A: DERIVATION OF THE RELAXATION TIME

At zero temperature the distribution Eq. (53) reads

$$f_n(k) = f(E_{nk}) - \frac{eF\hbar}{m}k\tau_n(E_{nk})\delta(E_{nk} - E_F), \quad (\text{A1})$$

and Boltzmann Eq. (55) can be written as

$$\frac{eF\hbar}{m}k\delta(E_{nk} - E_F) = \sum_{n'} \sum_{k'} W_{n,n'}(k,k') [f_{n'}(k') - f_n(k)]. \quad (\text{A2})$$

We set Eqs. (A1) and (56) into Eq. (A2). We obtain

$$\begin{aligned} k\delta(E_{nk} - E_F) &= \sum_{n'} \sum_{k'} \frac{2\pi}{\hbar} |\langle n',k' | U | n,k \rangle|_{\text{av}}^2 \\ &\quad \times \delta(E_{nk} - E_{n'k'}) [k'\tau_{n'}(E_{n'k'})\delta(E_{n'k'} - E_F) \\ &\quad - k\tau_n(E_{nk})\delta(E_{nk} - E_F)]. \end{aligned} \quad (\text{A3})$$

We proceed similarly to the Q2D theory.²⁹ First, we multiply both sides of Eq. (A3) by k and sum over k . Second, on the left-hand side we replace \sum_k by $(L/2\pi) \int dk$ and integrate. Third, on the right-hand side we replace $\tau_n(E_{nk})\delta(E_{nk} - E_F)$ by $\tau_n(E_F)\delta(E_{nk} - E_F)$ and $\delta(E_{nk} - E_{n'k'})\delta(E_{nk} - E_F)$ by $\delta(E_{n'k'} - E_F)\delta(E_{nk} - E_F)$, which is justified due to the presence of $\delta(E_{nk} - E_F)$. We obtain the equation

$$\begin{aligned} \frac{mL}{\pi\hbar^2}k_n &= \sum_{n'} \sum_k \sum_{k'} \frac{2\pi}{\hbar} |\langle n,k | U | n',k' \rangle|_{\text{av}}^2 \delta(E_{nk} - E_F) \\ &\quad \times \delta(E_{n'k'} - E_F) [k^2\tau_n(E_F) - kk'\tau_{n'}(E_F)] \end{aligned} \quad (\text{A4})$$

and from Eq. (A4) eventually

$$\frac{m}{\pi\hbar^2}k_n = \frac{2\pi}{\hbar} \sum_{n'} K_{nn'} \tau_{n'}(E_F), \quad (\text{A5})$$

where $K_{nn'}$ is defined by Eq. (58). From Eq. (A5) we obtain the relaxation time Eq. (57).

APPENDIX B: GOLDEN RULE FOR SCATTERING BY IMPURITY DISORDER

If the scattering potential U is given by the impurity potential Eq. (5), then

$$|\langle n', k' | U | n, k \rangle|_{\text{av}}^2 = |\langle n', k' | \sum_{i=1}^{N_I} \gamma \delta(x - x_i) \delta(y - y_i) | n, k \rangle|_{\text{av}}^2. \quad (\text{B1})$$

Since the impurities are positioned at random, Eq. (B1) can be readily simplified as

$$|\langle n', k' | U | n, k \rangle|_{\text{av}}^2 = \sum_{i=1}^{N_I} |\langle n', k' | \gamma \delta(x - x_i) \delta(y - y_i) | n, k \rangle|_{\text{av}}^2 \quad (\text{B2})$$

and the right-hand side of Eq. (B2) can be easily evaluated:

$$\begin{aligned} |\langle n', k' | U | n, k \rangle|_{\text{av}}^2 &= \frac{\gamma^2}{L^2} N_I \left[\frac{1}{N_I} \sum_{i=1}^{N_I} \chi_{n'}^2(y_i) \chi_n^2(y_i) \right]_{\text{av}} \\ &= \frac{\gamma^2 n_I}{LW} \left[1 - \frac{\delta_{nn'}}{2} \right], \end{aligned} \quad (\text{B3})$$

where $n_I = N_I/(WL)$ is the sheet impurity density. To obtain the right-hand side of Eq. (B3), we have replaced the term $\frac{1}{N_I} \sum_{i=1}^{N_I} \chi_{n'}^2(y_i) \chi_n^2(y_i)$ by integral $\frac{1}{W} \int_0^W \chi_{n'}^2(y) \chi_n^2(y) dy$. Setting Eq. (B3) into Eq. (58) we get expression (60).

APPENDIX C: GOLDEN RULE FOR SCATTERING BY EDGE ROUGHNESS

Assume first that the electrons are confined in the wire by the potential barriers of finite height. Specifically, if the wire edges are smooth, the electron Hamiltonian reads

$$H_0 = -\frac{\hbar^2}{2m} \left(\frac{\partial^2}{\partial x^2} + \frac{\partial^2}{\partial y^2} \right) + V_- \Theta(-y) + V_+ \Theta(y - W), \quad (\text{C1})$$

where V_- and V_+ is the height of the potential barrier at $y = 0$ and $y = W$, respectively, and Θ is the Heaviside step function. If the wire edges are rough, the Hamiltonian reads $H = H_0 + U$, where

$$\begin{aligned} U &= V_- [\Theta(-d(x) - y) - \Theta(-y)] \\ &\quad + V_+ [\Theta(y - h(x)) - \Theta(y - W)] \end{aligned} \quad (\text{C2})$$

is the perturbation potential due to the edge roughness, with $d(x)$ and $h(x) - W$ being the fluctuations of the edges (see Fig. 1). Now we also assume that $|d(x)| \ll W$ and $|h(x) - W| \ll W$ and we approximate Eq. (C2) as

$$U = -V_- d(x) \delta(-y) - V_+ [h(x) - W] \delta(y - W). \quad (\text{C3})$$

Then

$$\begin{aligned} |\langle n', k' | U | n, k \rangle|_{\text{av}}^2 &= \sum_{\beta=\pm} \frac{V_\beta^2}{L^2} \left| \int_0^L dx \int_0^W dy e^{i(k-k')x} \chi_{n'}(y) \chi_n(y) d_\beta(x) \delta_\beta(y) \right|_{\text{av}}^2, \end{aligned} \quad (\text{C4})$$

where $d_+(x) \equiv h(x) - W$, $d_-(x) \equiv d(x)$, $\delta_+(y) \equiv \delta(y - W)$, and $\delta_-(y) \equiv \delta(y)$. If we integrate in Eq. (C4) over the variable y and then use the limit

$$\lim_{V_- \rightarrow \infty} V_- \chi_n^2(0) = \lim_{V_+ \rightarrow \infty} V_+ \chi_n^2(W) = \frac{\hbar^2 \pi^2 n^2}{mW^3} \equiv A_n, \quad (\text{C5})$$

both terms in the sum on the right-hand side of Eq. (C4) can be rewritten into the form

$$\frac{A_n A_{n'}}{L^2} \int_0^L dx_1 \int_0^L dx_2 e^{i(k-k')(x_1-x_2)} \langle d_\beta(x_1) d_\beta(x_2) \rangle, \quad (\text{C6})$$

where the angle brackets $\langle \dots \rangle$ symbolize the ensemble averaging (instead of the symbol av) and $\langle d_\beta(x_1) d_\beta(x_2) \rangle$ is the roughness-correlation function. The correlation function depends on only the distance $|x_1 - x_2|$, so we rewrite it as

$$\langle d_\beta(x_1) d_\beta(x_2) \rangle = \delta_\beta^2 F_\beta(|x_1 - x_2|), \quad (\text{C7})$$

where $F_\beta(|x_1 - x_2|)$ is the normalized correlation function and δ_+ and δ_- are the root mean squares of the randomly fluctuating functions $d_+(x)$ and $d_-(x)$, respectively. We introduce the variable $x_3 = x_1 - x_2$ and simplify Eq. (C6) as

$$\begin{aligned} \frac{A_n A_{n'}}{L^2} \delta_\beta^2 \int_0^L dx_2 \int_{-x_2}^{L-x_2} dx_3 e^{i(k-k')x_3} F_\beta(|x_3|) \\ \simeq \frac{A_n A_{n'}}{L} \delta_\beta^2 \int_{-\infty}^{\infty} dx_3 e^{i(k-k')x_3} F_\beta(|x_3|). \end{aligned} \quad (\text{C8})$$

To obtain the second line in Eq. (C8), we have replaced the limits $L - x_2$ and $-x_2$ in the first line by ∞ and $-\infty$, respectively. Except for very small x_2 , such replacement is justified because $F_\beta(|x_3|)$ decays with increasing x_3 to zero on the distance (correlation length) much smaller than L .

Eq. (C4) can now be expressed as

$$|\langle n', k' | U | n, k \rangle|_{\text{av}}^2 = \sum_{\beta=\pm} \frac{A_n A_{n'}}{L} \delta_\beta^2 \mathcal{F}_\beta(|k - k'|), \quad (\text{C9})$$

where

$$\mathcal{F}_\beta(q) = \int_{-\infty}^{\infty} e^{iqx_3} F_\beta(x_3) dx_3 \quad (\text{C10})$$

is the Fourier transform of $F_\beta(x_3)$. Assuming the same randomness at both edges we can put

$$\delta_\pm = \delta, \quad F_\pm(x_3) = F(x_3), \quad \mathcal{F}_\pm(q) = \mathcal{F}(q), \quad (\text{C11})$$

i.e., we skip the indices \pm . We set Eqs. (C11) into Eq. (C9) and we replace the symbol $\sum_{\beta=\pm}$ in Eq. (C9) by factor of 2.

Finally, we set Eq. (C9) into Eq. (58). Performing a summation over k and k' we obtain the matrix elements $K_{nn'}$ in the form of Eq. (64).

*martin.mosko@savba.sk

- ¹Y. Imry, *Introduction to Mesoscopic Physics* (Oxford University Press, Oxford, UK, 2002).
- ²S. Datta, *Electronic Transport in Mesoscopic Systems* (Cambridge University Press, Cambridge, UK, 1995).
- ³P. A. Mello and N. Kumar, *Quantum Transport in Mesoscopic Systems* (Oxford University Press, Oxford, UK, 2004).
- ⁴L. Saminadayar, C. Bäuerle, and D. Mailly, in *Encyclopedia of Nanoscience and Nanotechnology*, edited by H. S. Nalwa (American Scientific, Valencia, CA, 2004), Vol. 3, pp. 267–285.
- ⁵P. Mohanty, E. M. Q. Jariwala, and R. A. Webb, *Phys. Rev. Lett.* **78**, 3366 (1997).
- ⁶H. Tamura and T. Ando, *Phys. Rev. B* **44**, 1792 (1991).
- ⁷M. Cahay, M. McLennan, and S. Datta, *Phys. Rev. B* **37**, 10125 (1988).
- ⁸A. García-Martín, J. A. Torres, J. J. Sáenz, and M. Nieto-Vesperinas, *Phys. Rev. Lett.* **80**, 4165 (1998).
- ⁹A. Garcia-Martin, F. Scheffold, M. Nieto-Vesperinas, and J. J. Saenz, *Phys. Rev. Lett.* **88**, 143901 (2002).
- ¹⁰J. Feilhauer and M. Moško, *Physica E* **40**, 1582 (2008).
- ¹¹R. Landauer, *IBM J. Res. Dev.* **1**, 223 (1957); *Philos. Mag.* **21**, 863 (1970).
- ¹²P. A. Mello and A. D. Stone, *Phys. Rev. B* **44**, 3559 (1991).
- ¹³P. A. Lee and A. D. Stone, *Phys. Rev. Lett.* **55**, 1622 (1985); I. Travěnek, *Phys. Rev. B* **69**, 033104 (2004).
- ¹⁴P. A. Lee, A. D. Stone, and H. Fukuyama, *Phys. Rev. B* **35**, 1039 (1987).
- ¹⁵P. W. Anderson, *Phys. Rev.* **109**, 1492 (1958).
- ¹⁶N. F. Mott and W. D. Twose, *Adv. Phys.* **10**, 107 (1961).
- ¹⁷J. A. Torres and J. J. Sáenz, *J. Phys. Soc. Jpn.* **73**, 2182 (2004).
- ¹⁸C. W. J. Beenakker, *Rev. Mod. Phys.* **69**, 731 (1997).
- ¹⁹P. Markoš, *Acta Physica Slovaca* **56**, 561 (2006).
- ²⁰J. A. Sánchez-Gil, V. Freilikher, A. A. Maradudin, and I. V. Yurkevich, *Phys. Rev. B* **59**, 5915 (1999).
- ²¹A. García-Martín and J. J. Sáenz, *Waves Random Complex Media* **15**, 229 (2005).
- ²²A. García-Martín and J. J. Sáenz, *Phys. Rev. Lett.* **87**, 116603 (2001).
- ²³A. García-Martín, J. A. Torres, J. J. Sáenz, and M. Nieto-Vesperinas, *Phys. Rev. Lett.* **80**, 4165 (1998).
- ²⁴L. S. Froufe-Pérez, M. Yépez, P. A. Mello, and J. J. Sáenz, *Phys. Rev. E* **75**, 031113 (2007).
- ²⁵J. A. Sánchez-Gil, V. Freilikher, I. Yurkevich, and A. A. Maradudin, *Phys. Rev. Lett.* **80**, 948 (1998).
- ²⁶A. García-Martín, J. A. Torres, J. J. Sáenz, and M. Nieto-Vesperinas, *Appl. Phys. Lett.* **71**, 1912 (1997).
- ²⁷K. Nikolic and A. MacKinnon, *Phys. Rev. B* **50**, 11008 (1994).
- ²⁸T. Ando and H. Tamura, *Phys. Rev. B* **46**, 2332 (1992).
- ²⁹G. Fishman and D. Calecki, *Phys. Rev. B* **29**, 5778 (1984).
- ³⁰G. Fishman and D. Calecki, *Phys. Rev. Lett.* **62**, 1302 (1989).
- ³¹H. Akera and T. Ando, *Phys. Rev. B* **43**, 11676 (1991).
- ³²A. Cohen, Y. Roth, and B. Shapiro, *Phys. Rev. B* **38**, 12125 (1988).
- ³³G. Palasantzas and J. Barnas, *Phys. Status Solidi B* **211**, 671 (1999).
- ³⁴T. Ando, A. B. Fowler, and F. Stern, *Rev. Mod. Phys.* **29**, 5778 (1982).
- ³⁵Z. Tešanović, M. V. Jarić, and S. Maekawa, *Phys. Rev. Lett.* **57**, 2760 (1986).
- ³⁶P. W. Anderson, D. J. Thouless, E. Abrahams, and D. S. Fisher, *Phys. Rev. B* **22**, 3519 (1980).
- ³⁷D. J. Thouless, *Phys. Rev. Lett.* **39**, 1167 (1977).
- ³⁸P. Vagner, P. Markoš, M. Moško, and T. Schapers, *Phys. Rev. B* **67**, 165316 (2003).
- ³⁹M. Moško, P. Vagner, M. Bajdich, and T. Schapers, *Phys. Rev. Lett.* **91**, 136803 (2003).
- ⁴⁰F. G. Bass and I. M. Fuks, *Wave Scattering From Statistically Rough Surfaces* (Pergamon, New York, 1979).
- ⁴¹F. M. Izrailev and N. M. Makarov, *Phys. Stat. Sol. (c)* **0**, 3037 (2003).
- ⁴²At first glance it might seem that the scattering has to be weak if L is sufficiently small. However, the quasi-ballistic (not ballistic) regime is a meaningful concept only if the length L involves at least one edge step. Even one edge step can scatter strongly if the step size is large.
- ⁴³F. M. Izrailev, N. M. Makarov, and M. Rendón, *Phys. Rev. B* **73**, 155421 (2006).
- ⁴⁴All this is correct for weak impurities. If the impurities are not weak, the semiclassical Boltzmann result has to be modified by treating the single-impurity scattering nonperturbatively. See, e.g., M. Mosko and P. Vagner, *Phys. Rev. B* **59**, R10445 (1999).
- ⁴⁵K. Fuchs, *Proc. Cambridge Philos. Soc.* **34**, 100 (1938).
- ⁴⁶E. H. Sondheimer, *Adv. Phys.* **1**, 1 (1952).
- ⁴⁷C. Durkan and M. E. Welland, *Phys. Rev. B* **61**, 14215 (2000).
- ⁴⁸W. Steinhogel, G. Schindler, G. Steinlesberger, and M. Engelhardt, *Phys. Rev. B* **66**, 075414 (2002).
- ⁴⁹R. L. Graham, G. B. Alers, T. Mountsier, N. Shamma, S. Dhuey, S. Cabrini, R. H. Geiss, D. T. Read, and S. Peddeti, *Appl. Phys. Lett.* **66**, 042116 (2010).
- ⁵⁰H. S. Lee and J. B. Yoon, *J. Micromech. Microeng.* **15**, 2136 (2005).
- ⁵¹A. Voigt, M. Heinrich, K. Hauck, R. Mientus, G. Gruetzner, M. Topper, and O. Ehrmann, *Microelectron. Eng.* **89**, 503 (2005).
- ⁵²M. T. Bryan, D. Atkinson, and R. P. Cowburn, *J. Phys. Conf. Ser.* **17**, 40 (2005).